正电子概况XII

正电子技术在材料科学中的应用--- nanoparticles

叶邦角

核固体物理研究室

Laboratory of Nuclear Solid State Physics, USTC

Positron for Nano-particles

一. 纳米粒子

二. 纳米粒子嵌入

三. 纳米粒子在表面

一. 纳米粒子

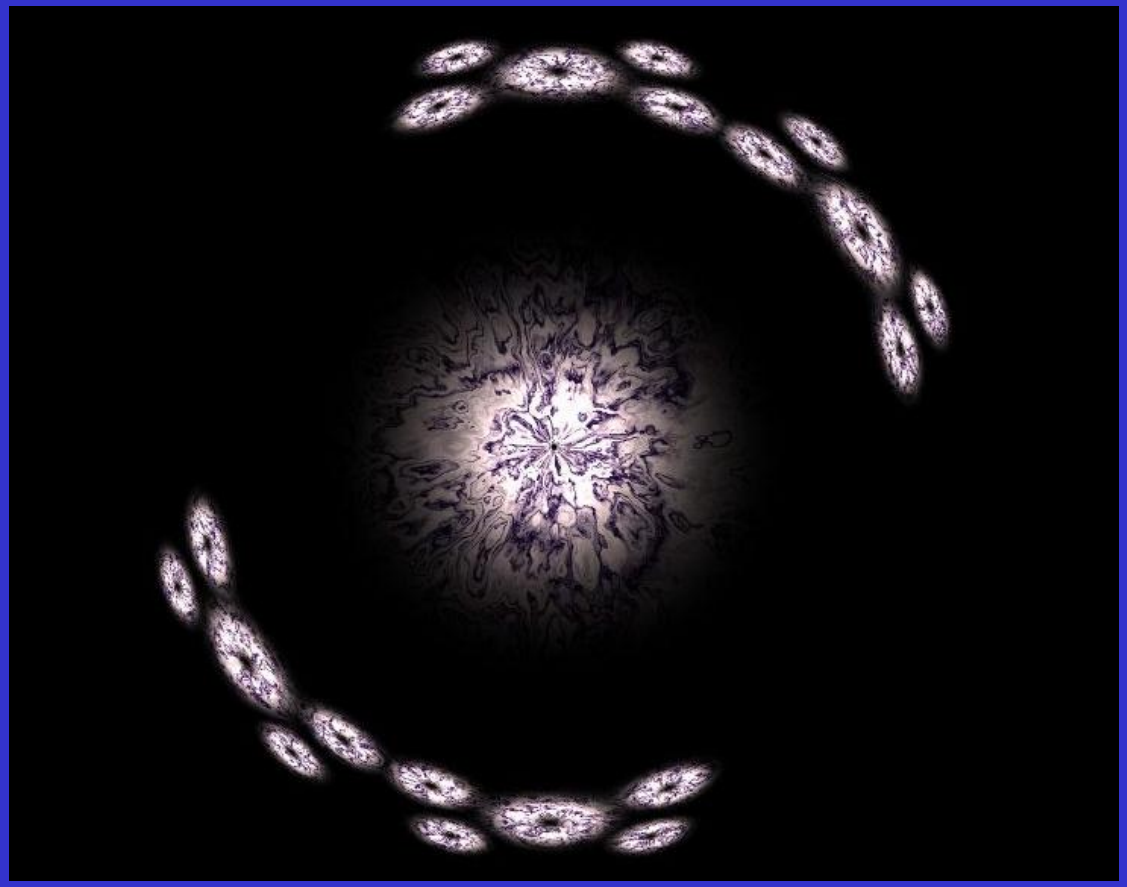

INSTITUTE OF PHYSICS PUBLISHING NANOTECHNOLOGY
Nanotechnology 15 (2004) 467–472 PII: S0957-4484(04)62779-6

Trapping of positrons at grain boundaries in nanoparticle systems

V Thakur, S B Shrivastava and M K Rathore

School of Studies in Physics, Vikram University, Ujjain (MP)-456010, India

E-mail: vandanathakur1@rediffmail.com

Abstract

The positron annihilation in nanoparticle materials has been discussed in terms of the thermal diffusion of positrons at grain surfaces and trapping at the grain interfaces and interfacial defects. The diffusion trapping model has been applied to obtain the mean lifetime of positrons as a function of grain size and temperature and the *S*-parameter of the annihilation radiation as a function of grain size in Ag, Nb, Zn–Al and Zn–Al–Mg nanocrystallites. The calculated mean positron lifetimes have beencompared with the available experimental results.

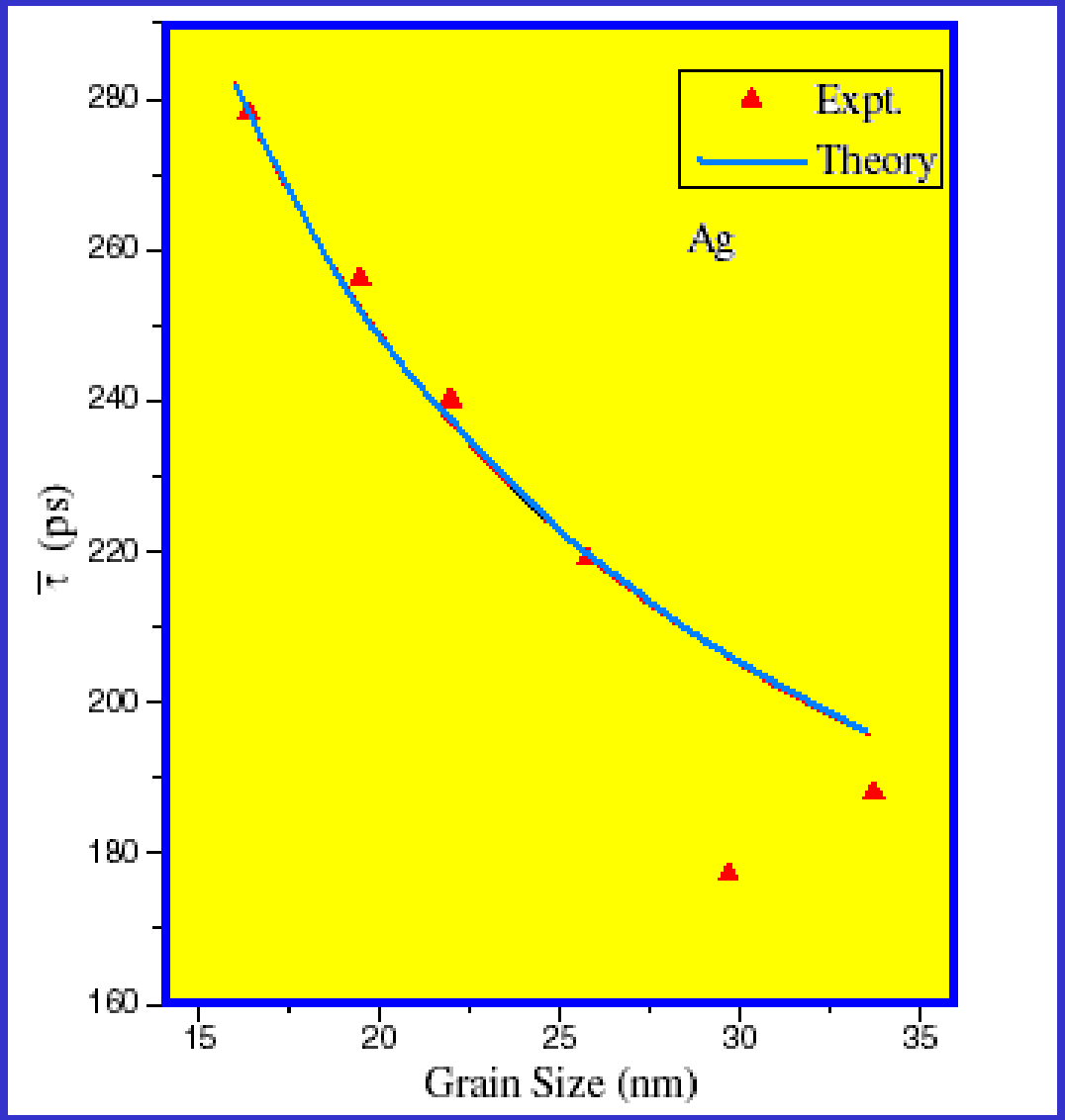

- Comparison with the experimental results of the calculated mean positron lifetime in Ag nanocrystallites as a function of grain size.

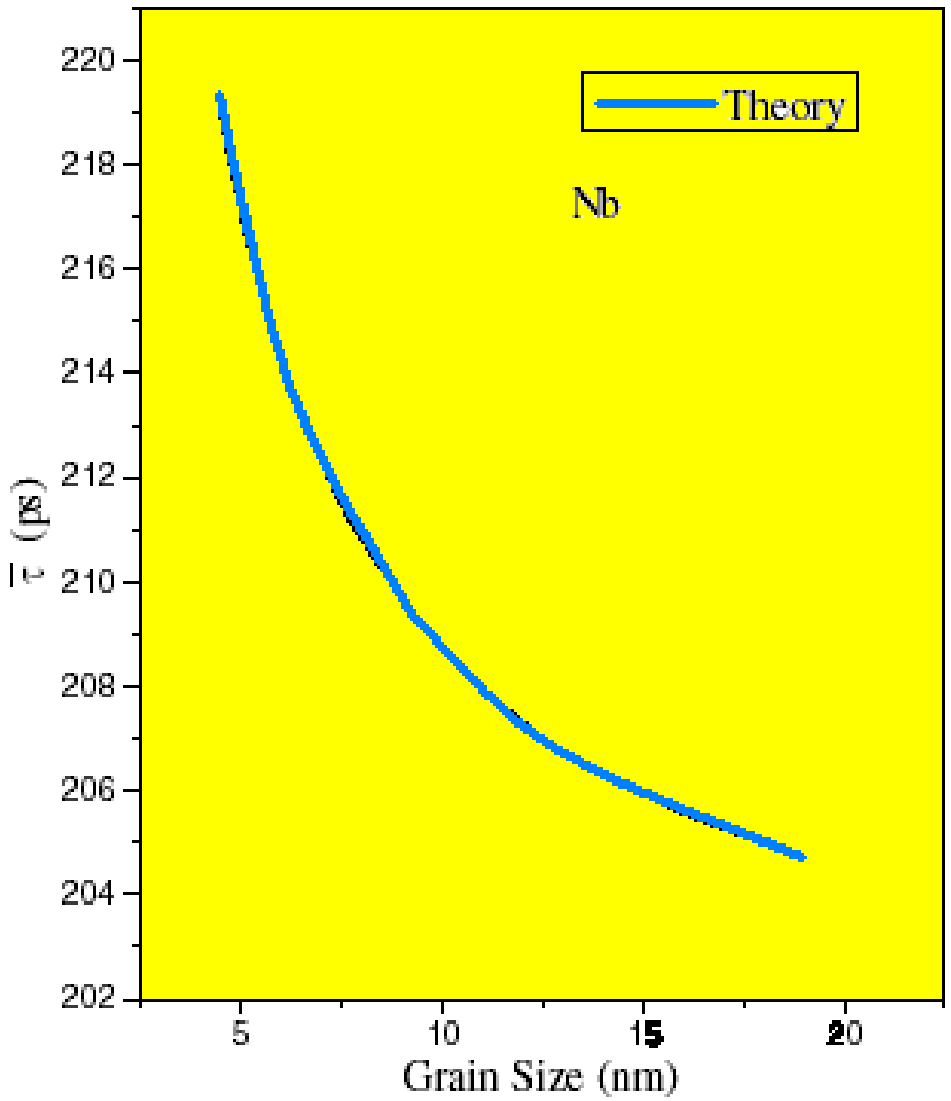

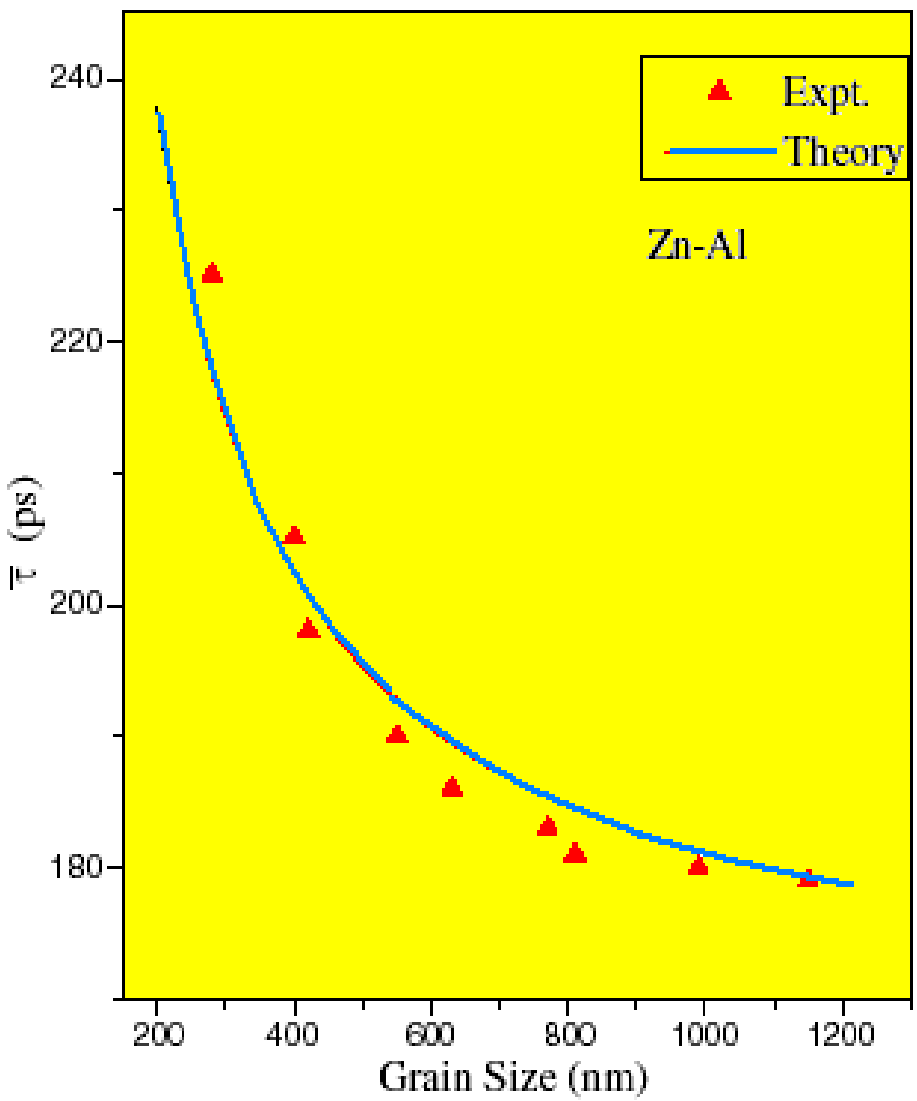

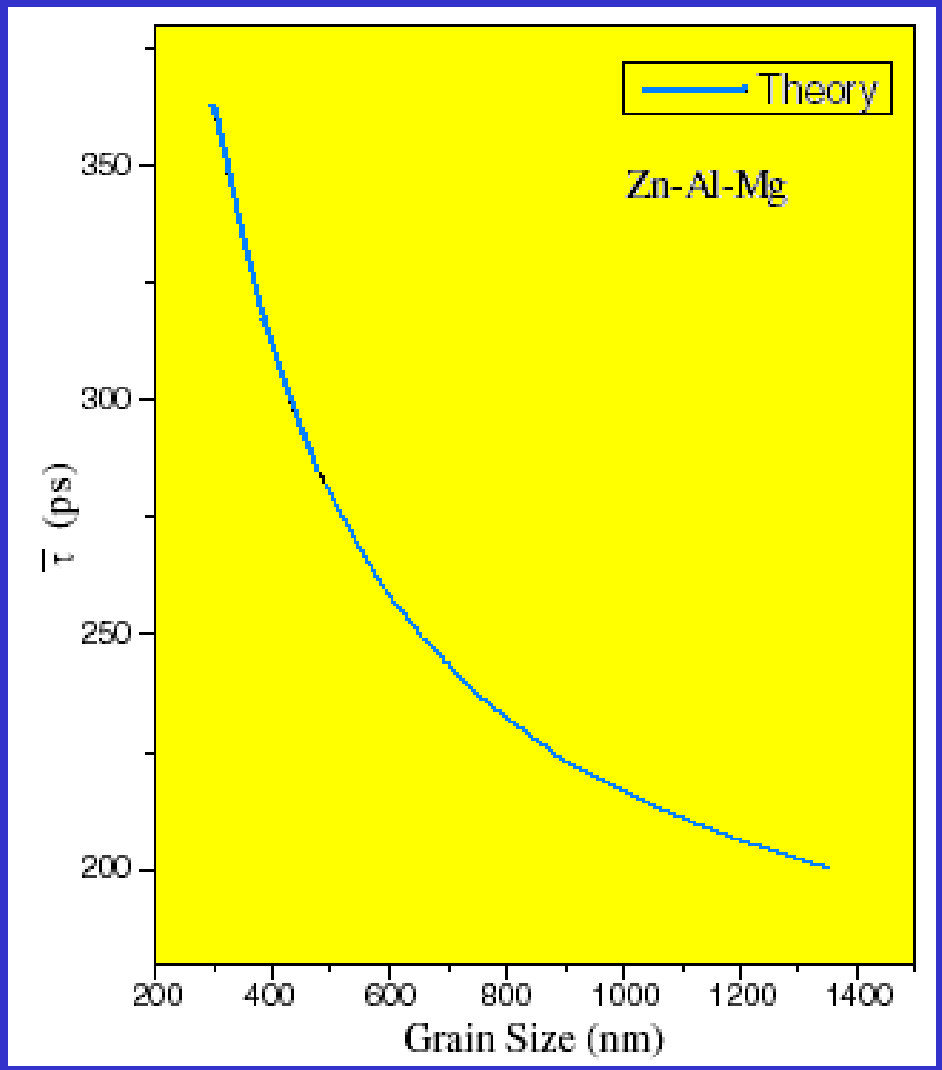

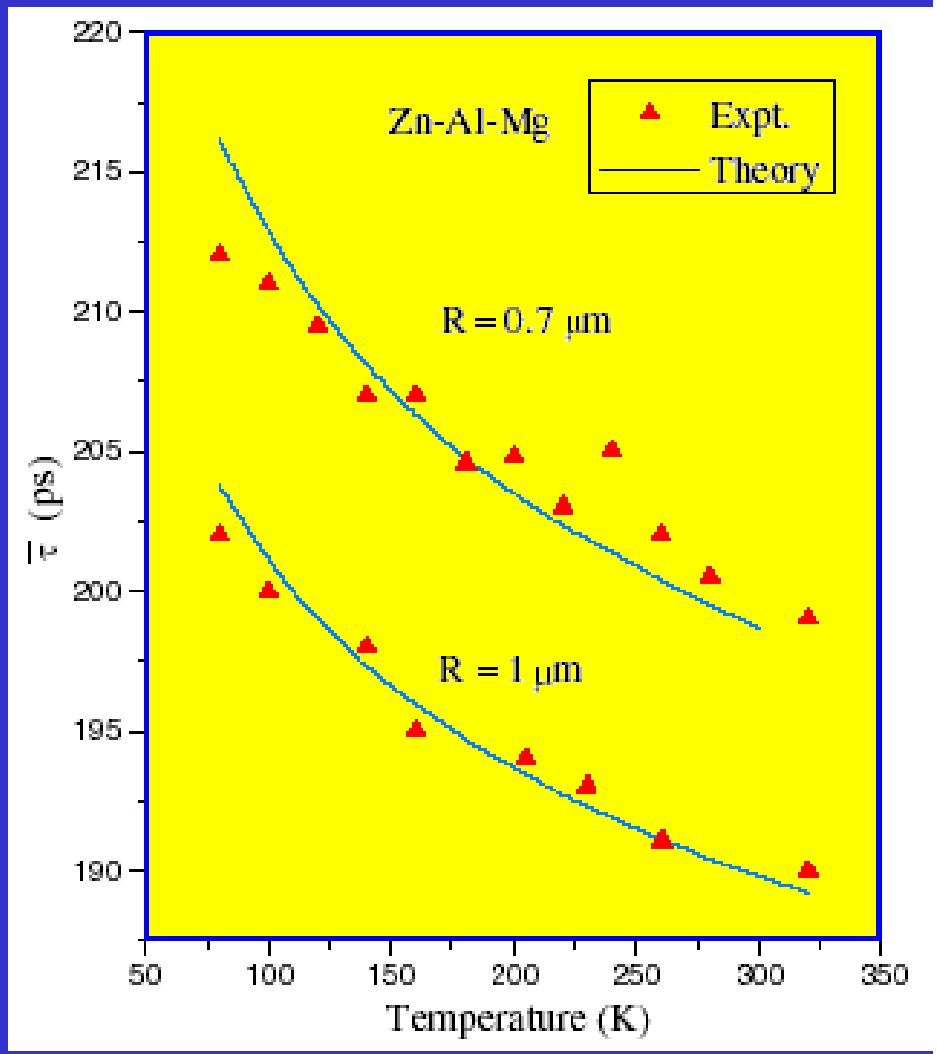

S-参数

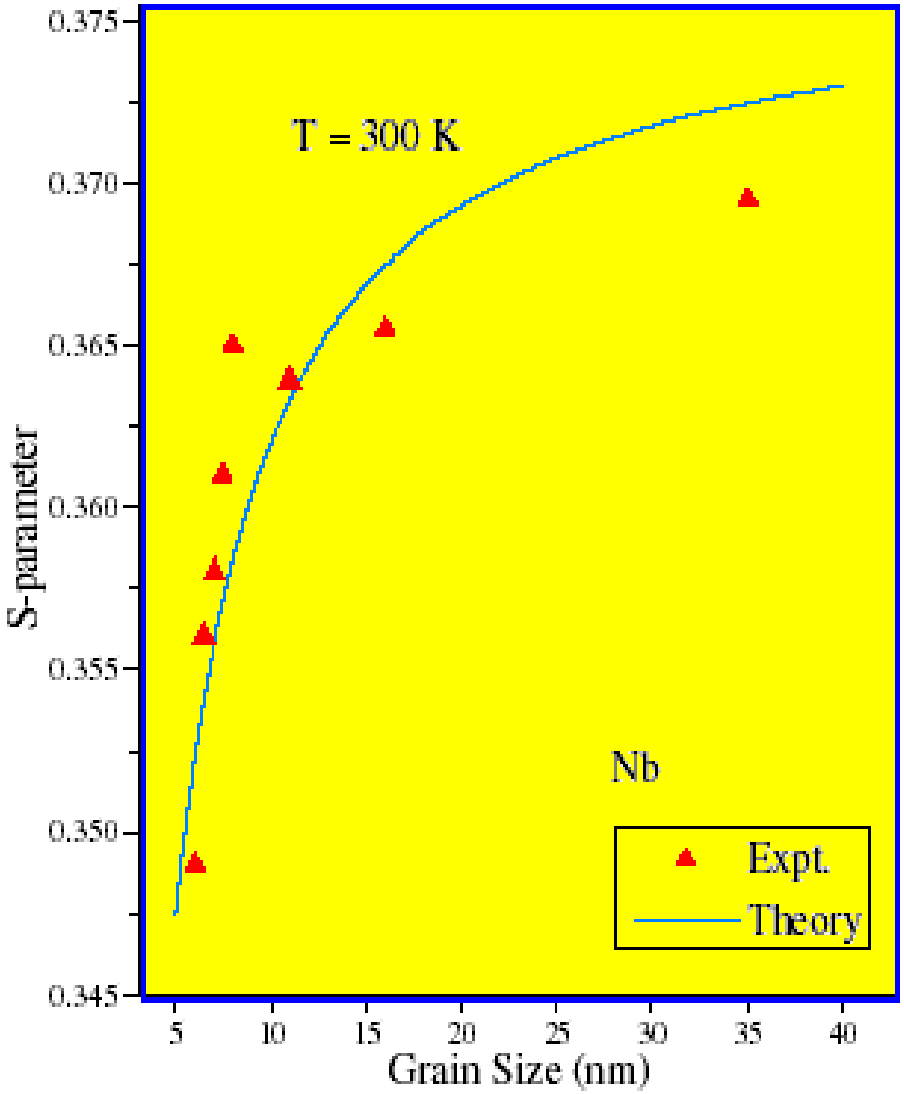

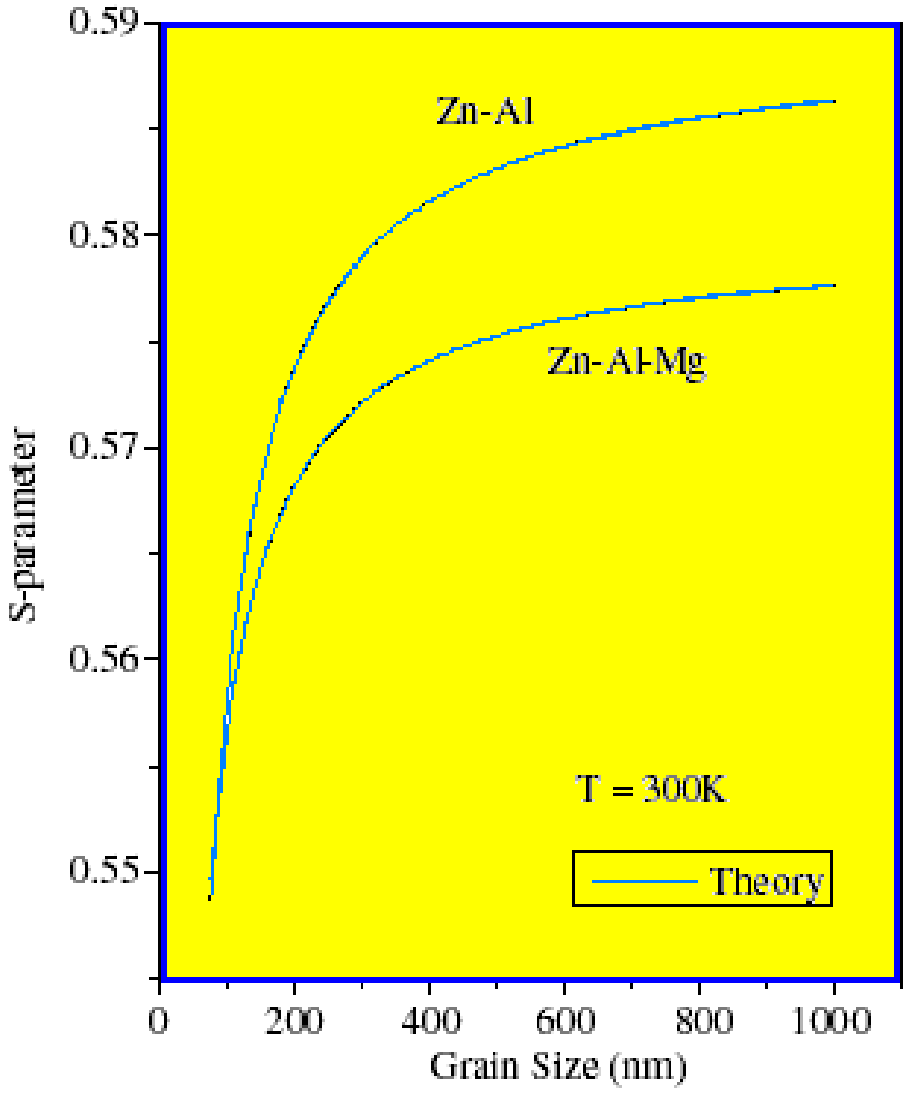

Conclusions

(1)The mean positron lifetime has been found to decrease with an increase in the size of the grains. At large grain size, comparable to the diffusion length, annihilation occurs in the bulk state.

(2) The diffusion coefficient $D+$ could be described by the relation $D_+ = D_0 T^{-1/2}$. The variation of the S-parameter in nanocrystalline samples suggests that the material undergoes significant changes at low grain size.

JOURNAL OF APPLIED PHYSICS VOLUME 93, NUMBER 10

Positron lifetime spectroscopic studies of nanocrystalline $ZnFe_2O_4$

P. M. G. Nambissan[a)]
Nuclear and Atomic Physics Division, Saha Institute of Nuclear Physics, 1/AF Bidhannagar, Kolkata 700 064, India

C. Upadhyay and H. C. Verma
Department of Physics, Indian Institute of Technology, Kanpur 208 016, India

(Received 9 December 2002; accepted 6 March 2003)

TABLE I. Grain size (d_c) and lattice parameter (a) of the $ZnFe_2O_4$ samples as estimated from the x-ray diffraction data.

Samples	d_c (nm)	a (Å)
CTR Series	Bulk	8.448
	14	8.448
	9	8.432
	7	8.356
	6	8.343
	5	8.267
CER Series	Bulk	8.448
HTR Series	6	8.438
	4	8.437

TABLE II. Positron lifetime parameters of nanocrystalline $ZnFe_2O_4$.

CTR samples	d_c (nm)	τ_1 (ps)	τ_2 (ps)	τ_3 (ns)	I_1 (%)	I_2 (%)	I_3 (%)	τ_m (ps)	τ_b (ps)
	Bulk	129	248	···	65.1	34.9	···	174	155
	14	145	380	1.86	49.0	50.4	0.6	274	
	9	153	398	2.64	52.1	47.1	0.8	288	
	7	150	397	2.24	47.7	51.5	0.8	293	
	6	142	386	2.20	40.2	58.9	0.9	297	
	5	143	384	1.89	44.2	54.8	1.0	293	
CER sample	Bulk	130	253	···	60.9	39.1	···	178	161
HTR samples	6	156	442	4.05	55.2	43.7	1.1	326	
	4	145	371	6.13	52.0	46.1	1.9	363	

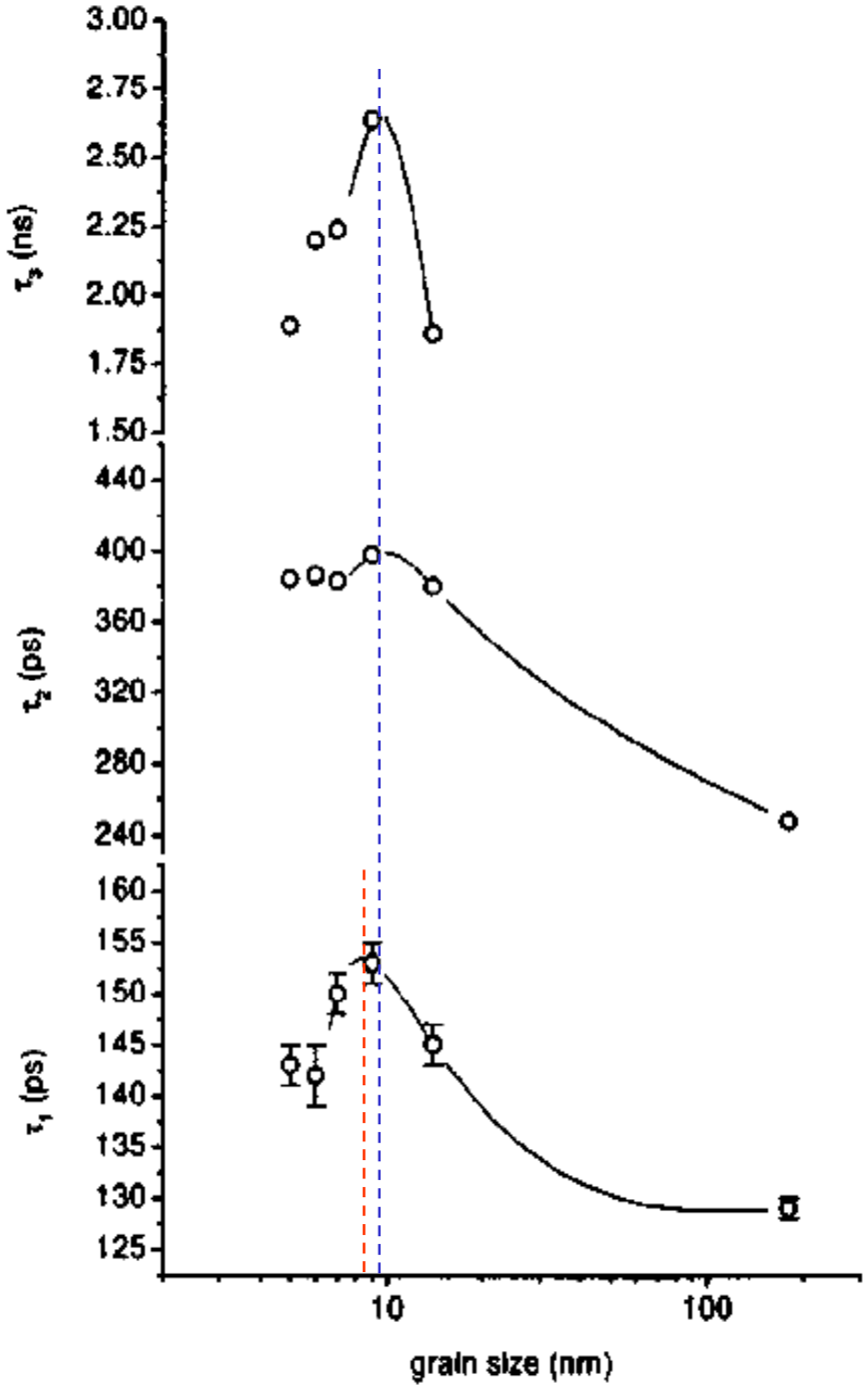

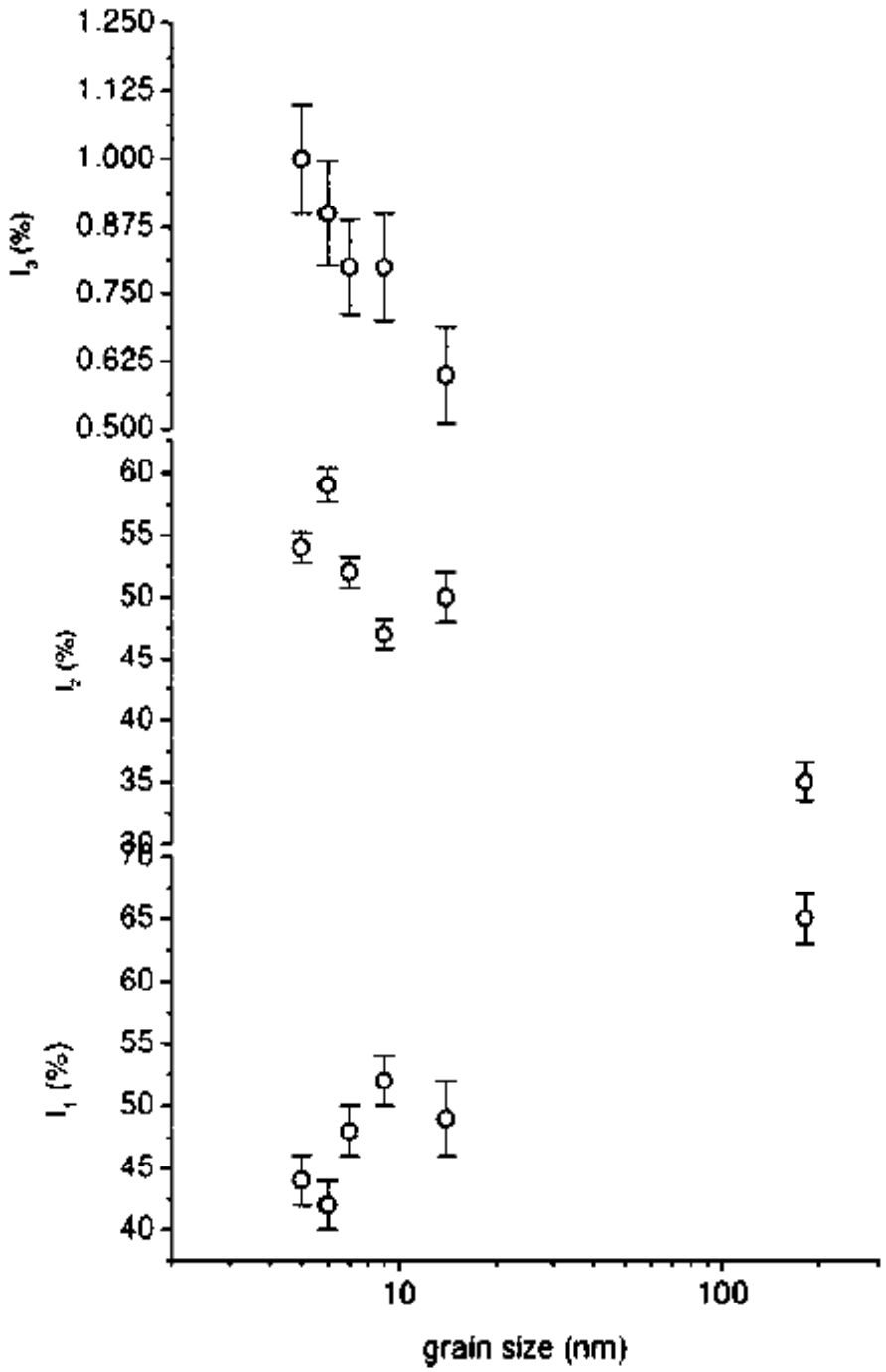

PHYSICAL REVIEW B **71**, 064105 (2005)

Positron annihilation lifetime changes across the structural phase transition in nanocrystalline Fe_2O_3

S. Chakrabarti* and S. Chaudhuri†
Department of Materials Science, Indian Association for the Cultivation of Science, Jadavpur, Kolkata 700032, India

P. M. G. Nambissan‡
Nuclear and Atomic Physics Division, Saha Institute of Nuclear Physics, 1/AF Bidhannagar, Kolkata 700064, India
(Received 14 September 2004; published 22 February 2005)

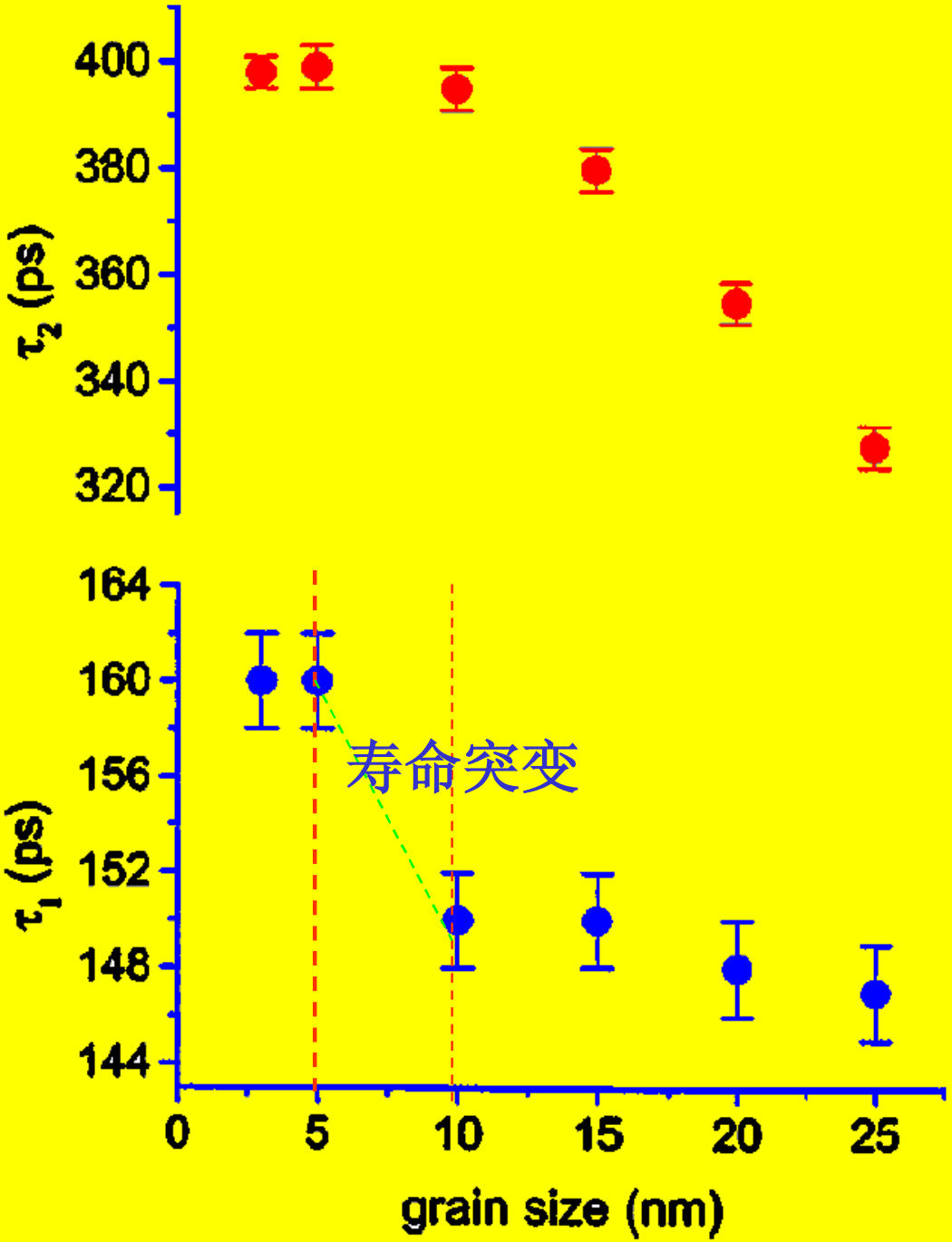

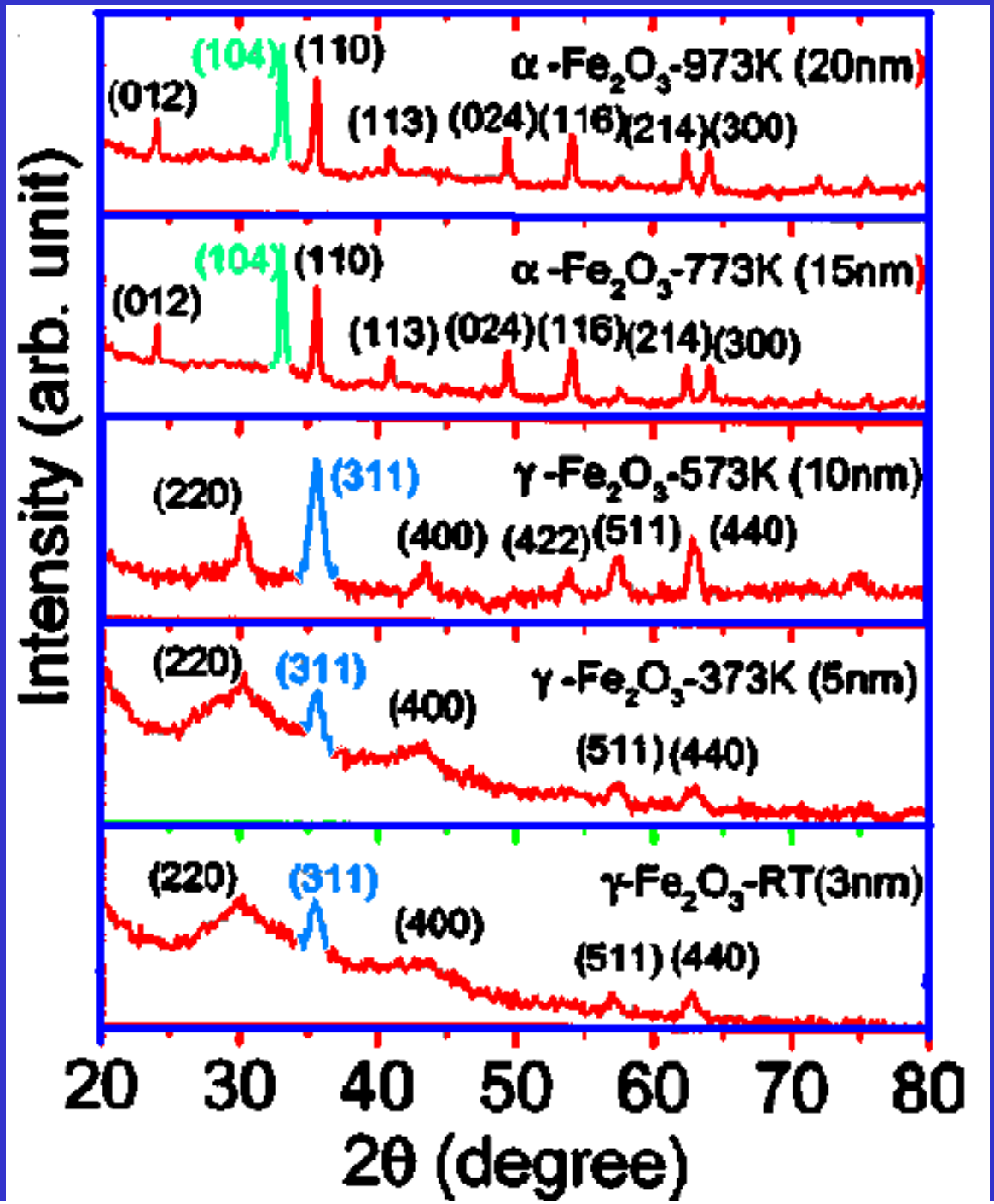

X-ray diffraction patterns of the Fe_2O_3 samples, indicating the characteristic peaks of the γ and α phases.

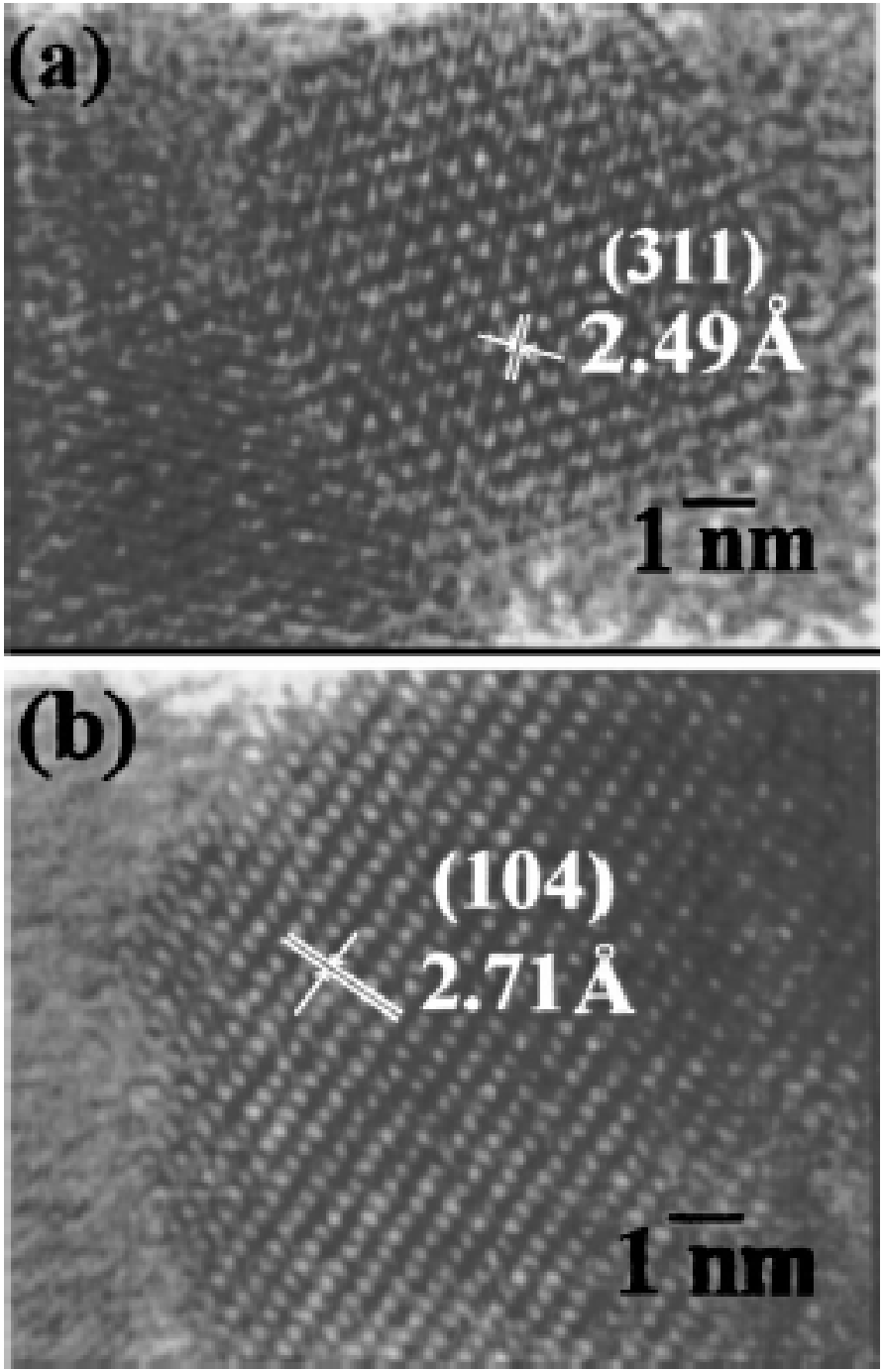

High-resolution transmission electron micrographs of (α)γ-Fe_2O_3 and (b) α-Fe_2O_3, indicating the lattice fringes.

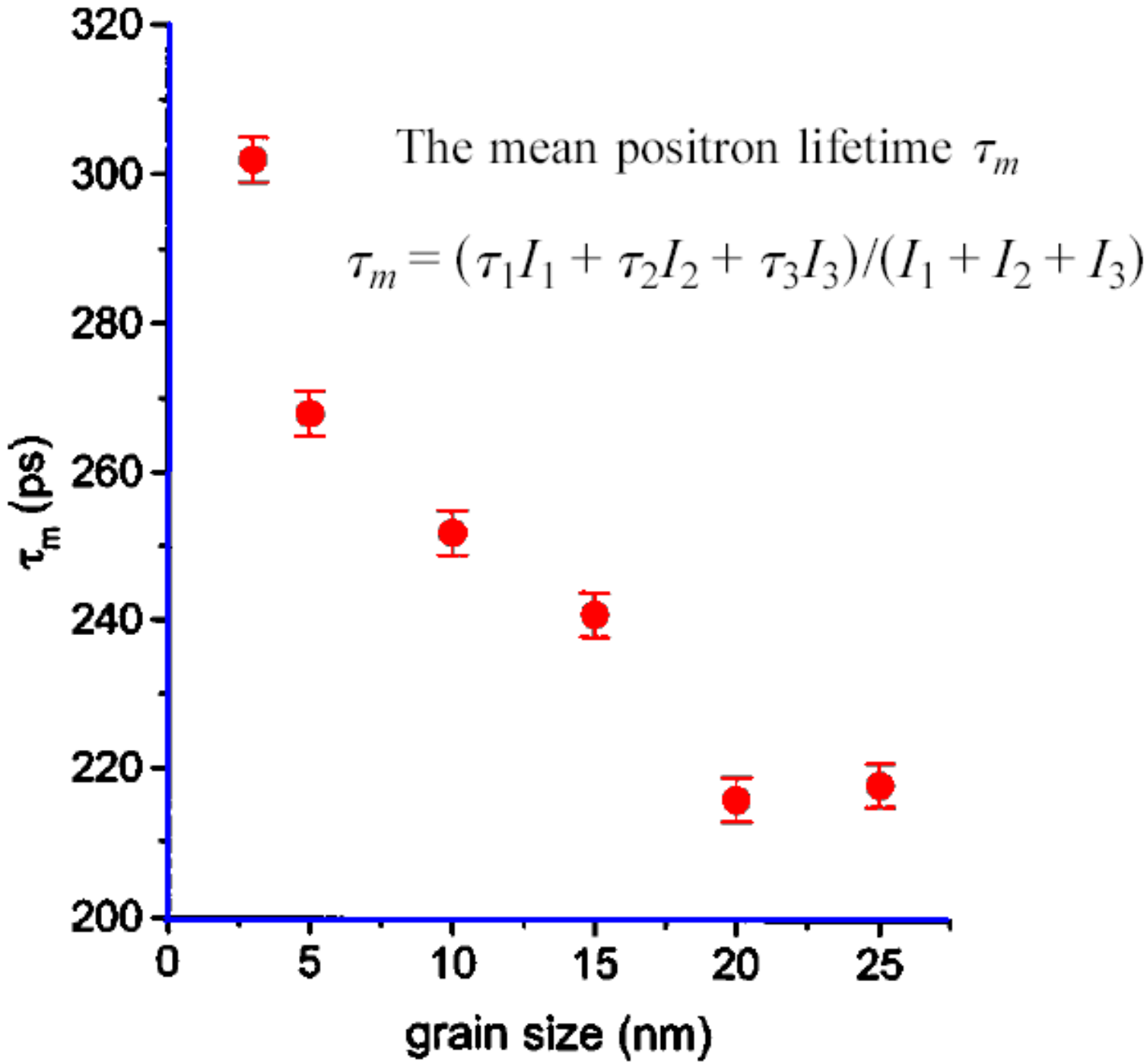

PHYSICAL REVIEW B **71**, 024115 (2005)

Positron annihilation studies of some anomalous features of $NiFe_2O_4$ nanocrystals grown in SiO_2

S. Chakraverty,* Subarna Mitra,† and K. Mandal‡
C.K. Majumdar Laboratory, S.N. Bose National Centre for Basic Sciences, Block JD, Sector III, Salt Lake, Kolkata 700098, India

P. M. G. Nambissan§
Nuclear an ... *064, India*

Department of Phy ... *ata 700009, India*
(Re ... 5)

TABLE I. The temperature and duration of heat treatment used for growing $NiFe_2O_4$ nanoparticles of different sizes (as obtained from XRD) in the SiO_2 matrix. The lattice parameter obtained for the different samples are also given.

Temperature (K)	Duration of annealing (h)	Grain size (nm)	Lattice constant (Å)
973	2	3.5	8.16
1073	1	4.8	8.19
1173	1	5.6	8.22
1273	2	6.8	8.25
1273	5	15.0	8.26
1273	24	25.0	8.27
1273	98	40.0	8.28

TABLE II. Positron lifetimes and their intensities in samples of $NiFe_2O_4$ nanocrystals of different mean grain sizes and grown in SiO_2. The values obtained for the reference SiO_2 are also presented. Typical errors in the lifetimes and intensities are 2 ps, 5 ps, 0.8 ns, 2%, 2%, and 0.1–1.0%, respectively.

Grain size (nm)	τ_1 (ps)	τ_2 (ps)	τ_3 (ns)	I_1 (%)	I_2 (%)	I_3 (%)
3.5	142	432	1.29	52.0	45.1	2.9
4.8	133	406	1.08	50.6	45.2	4.2
5.6	131	392	1.13	50.8	46.2	3.0
6.8	143	420	1.43	56.1	41.7	2.2
15.0	139	416	1.50	54.0	43.3	2.7
25.0	137	400	1.76	55.8	38.5	5.7
40.0	133	400	1.64	51.5	38.9	9.6
SiO_2	116	370	1.62	50.1	27.2	22.7

JOURNAL OF APPLIED PHYSICS 97, 014301 (2005)

Positron annihilation lifetime and coincidence-gated Doppler broadening studies of FeS_2 nanostructures

S. Kar and S. Chaudhuri
Department of Materials Science, Indian Association for the Cultivation of Science, Jadavpur, Kolkata 700032, India

TABLE I. Positron lifetimes and intensities in the different samples of FeS_2 studied in this work. The typical errors in τ_1, τ_2, and τ_3 are 2 ps, 4 ps, and 0.08 ns and in I_1, I_2, and I_3 are 1.7%, 1.7%, and 0.05%, respectively.

Sample description	τ_1 (ps)	τ_2 (ps)	τ_3 (ns)	I_1 (%)	I_2 (ps)	I_3 (%)	τ_m (ps)
Bulk	132	296	1.000	46.6	52.8	0.6	224
Nanogranular sample	141	322	1.292	45.1	54.2	0.7	247
Nanoribbons	122	324	1.046	36.4	61.4	2.2	266
Oxidized nanoribbons	186	355	2.120	50.8	48.9	0.3	274
Nanorods	135	340	1.260	37.4	61.4	1.2	274
Nanowires+nanotubes	149	374	1.396	44.0	50.0	6.0	336

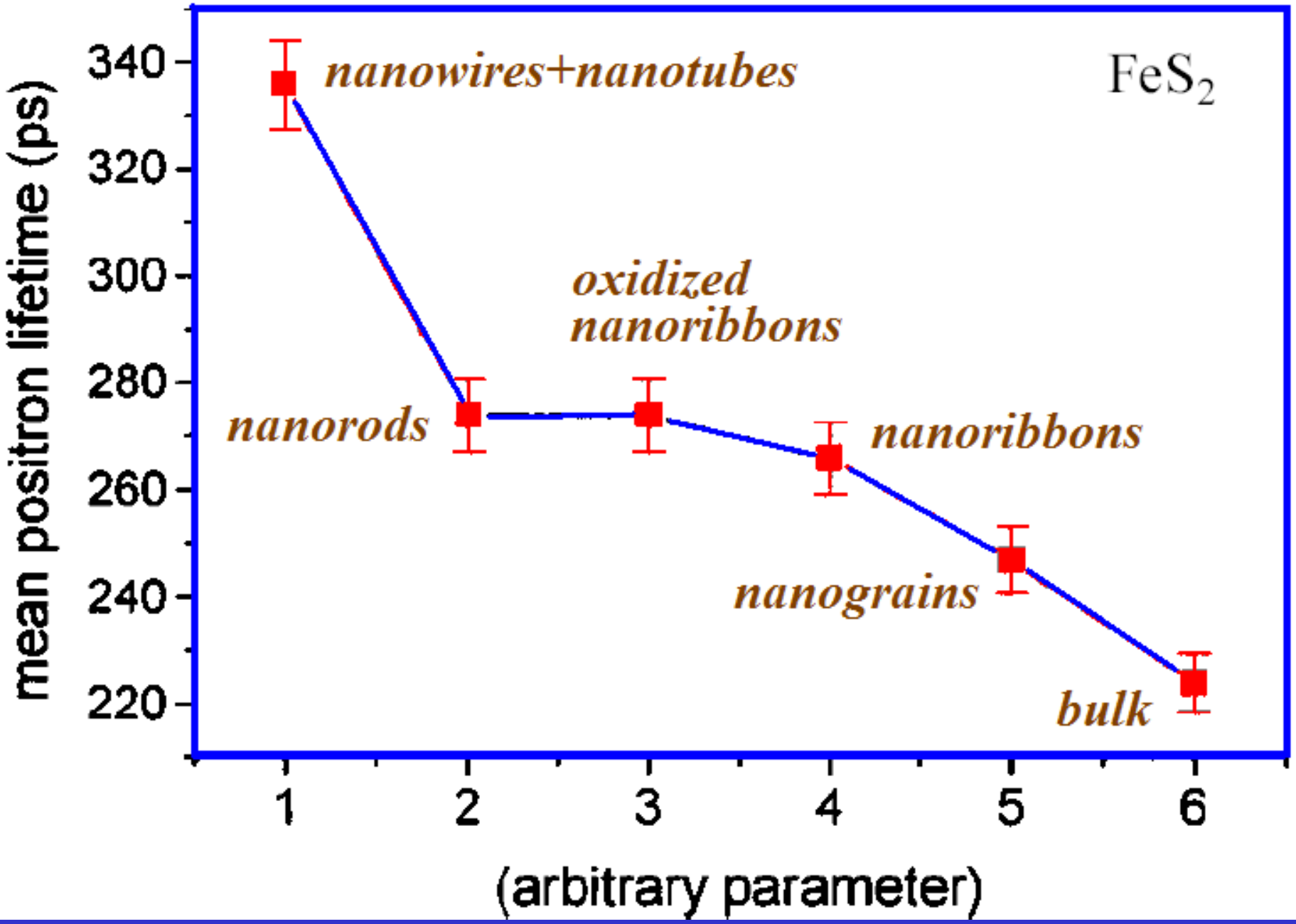

二. 纳米粒子嵌入

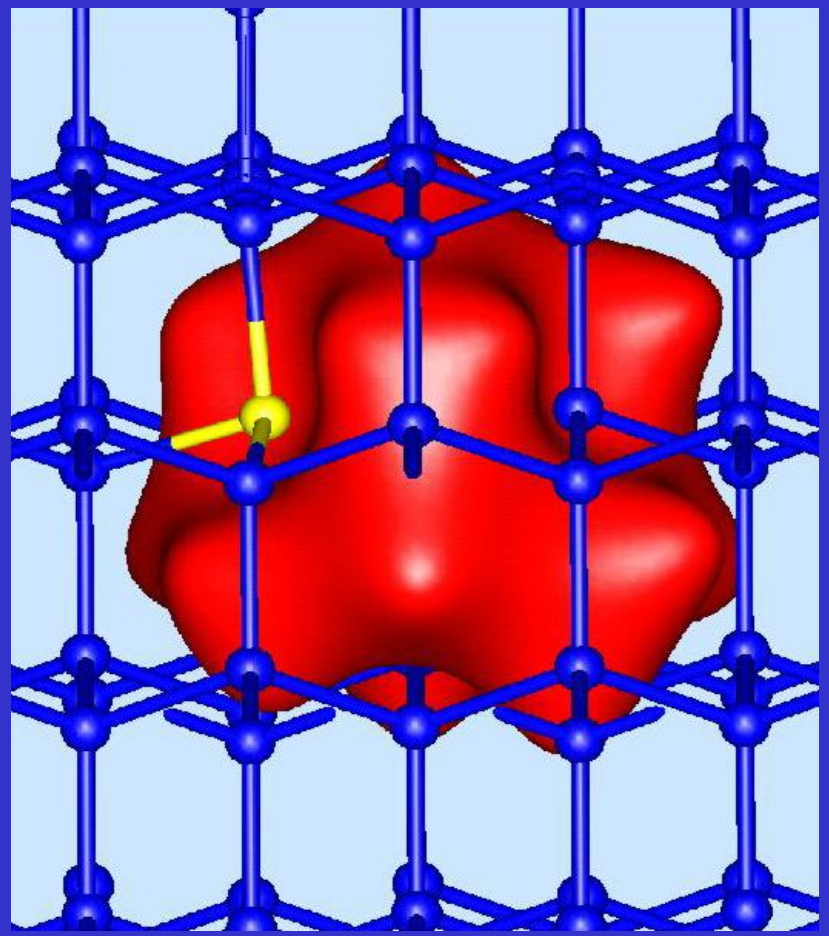

1. The minimum radius of particles that may trap positrons

$$r[A^{o}] = \frac{3.1}{\sqrt{\Delta A_{+}(eV)}}$$

Cu-Fe system:

Positron Affinities: A_{+}(Fe):-3.8eV, A_{+}(Cu):-4.5eV

$$r[A^{o}] = \frac{3.1}{\sqrt{0.7(eV)}} = 3.7$$

The 15 Cu atom particle has an effective radius of 3.5 ^{o}A.

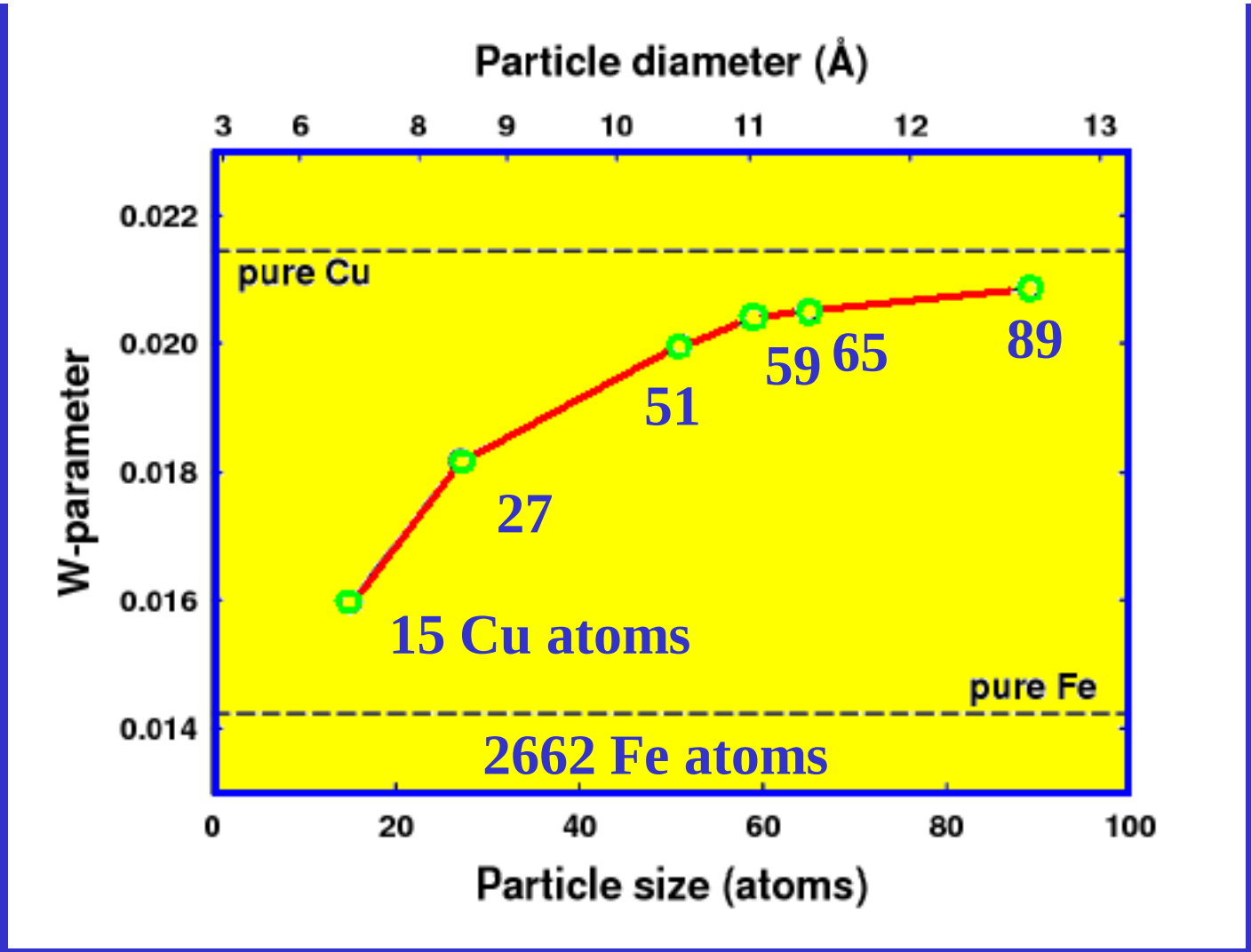

- One can deduce an important piece of information that PA methods can be used to measure the size of Cu particles in the range from 7Aº to 13Aº and PA can be used to monitor early precipitation stages of Cu in Fe.

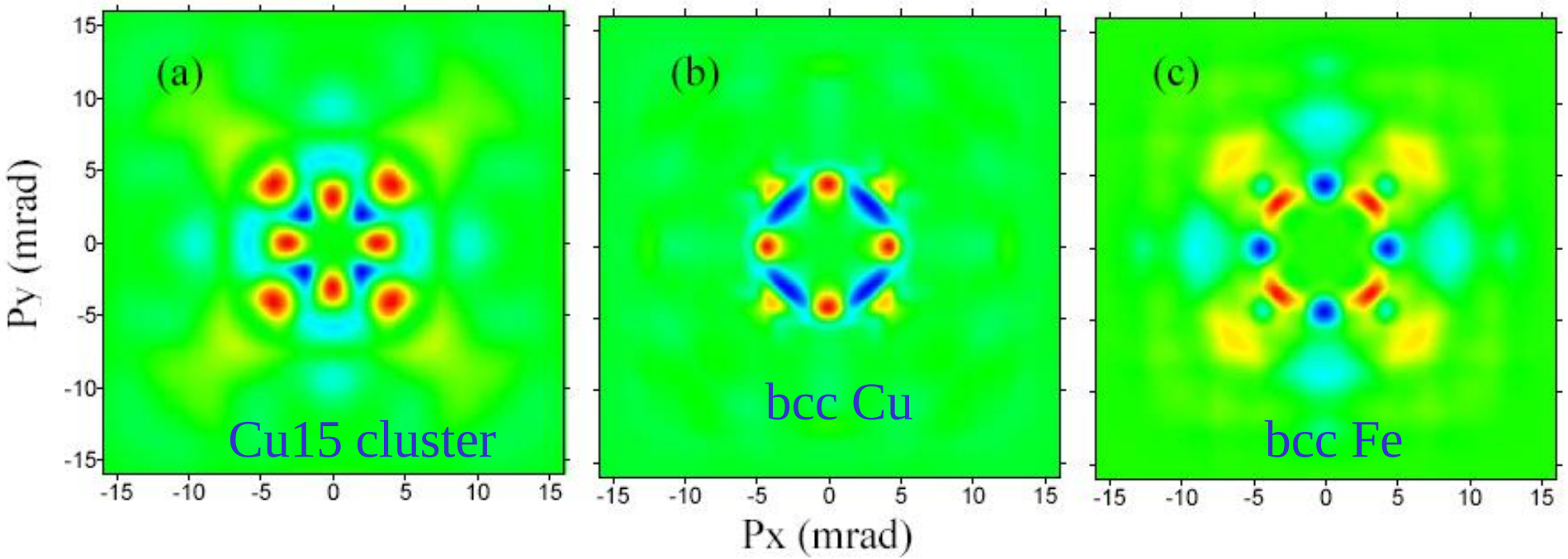

- Anisotropies of electron momentum density distribution in embedded Cu15 cluster sampled by quantum-confined positron, in comparison with those in bcc Cu (b) and bcc Fe (c).

J. Phys.: Condens. Matter **1** (1989) 6081-6093.

Positron affinities for elemental metals

M J Puska, P Lanki and R M Nieminen

Laboratory of Physics, Helsinki University of Technology
02150 Espoo, Finland

Li -7.36	Be -3.11												
Na -7.12	Mg -6.18											Al -4.41	Si -6.95
K -7.05	Ca -6.40	Sc -5.10	Ti -4.06	V -3.44	Cr -2.62	Mn -3.72	Fe -3.84	Co -4.18	Ni -4.46	Cu -4.81	Zn -5.24		Ge -6.69
Rb -6.98	Sr -6.41	Y -5.31	Zr -3.98	Nb -2.93	Mo -1.92	Tc -1.67	Ru -1.92	Rh -3.10	Pd -5.04	Ag -5.36	Cd -5.78		Sn -7.60
Cs -6.94	Ba -6.13	Lu -4.90	Hf -3.70	Ta -2.63	W -1.31	Re -0.97	Os -0.89	Ir -1.53	Pt -3.63	Au -4.59			Pb -5.56

The Zn precipitates bin Al, the critical radius is 5.4 a_0,. This means that precipitates should contain at least ~6 Zn atoms.

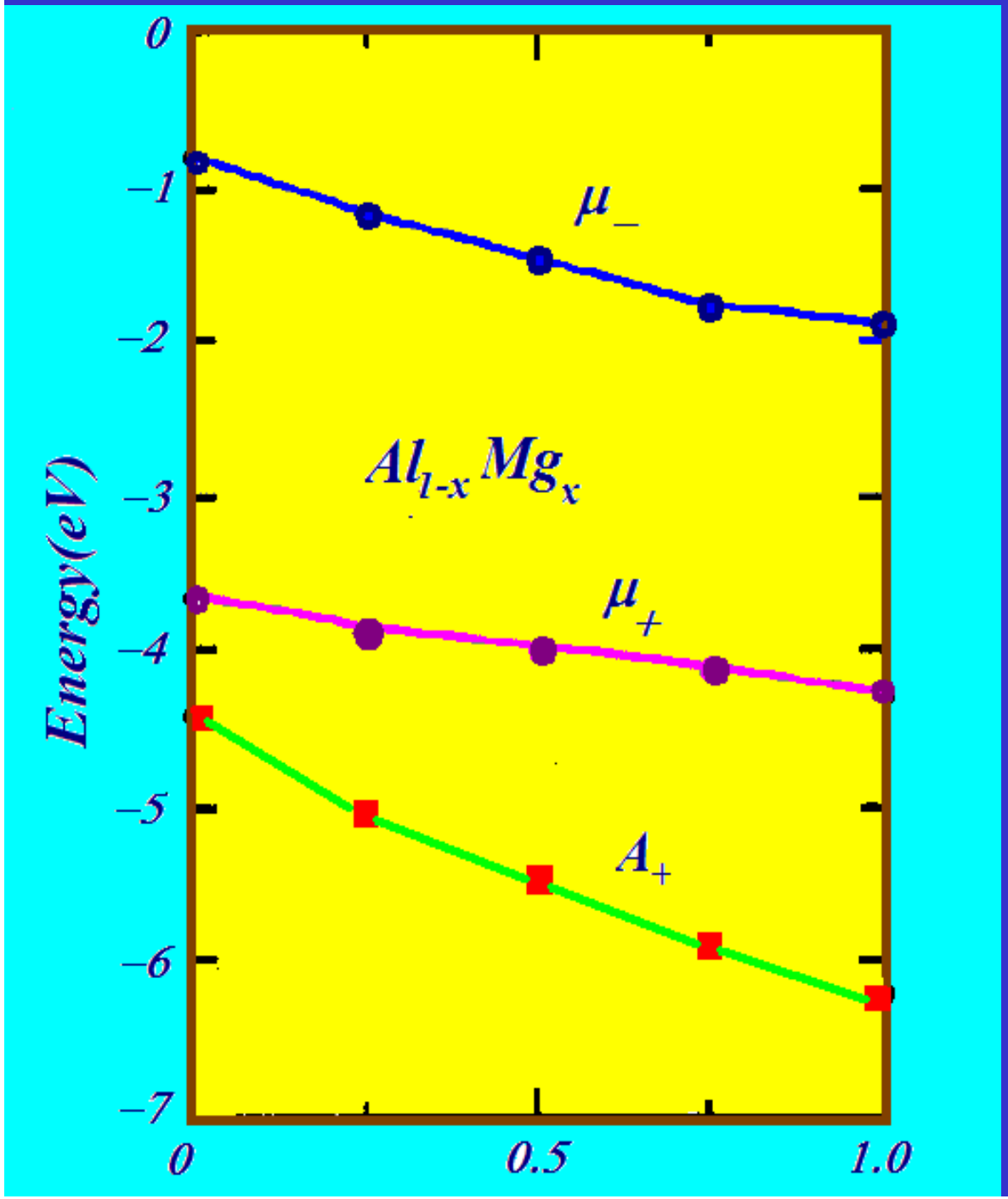

The electron (*m* -) and positron (*m*+)chemical potentials and the positron affinity (***A***$_+$)in $Al_{1-x}Mg_x$, as a function of the composition ***x*** .

2. Positron affinities

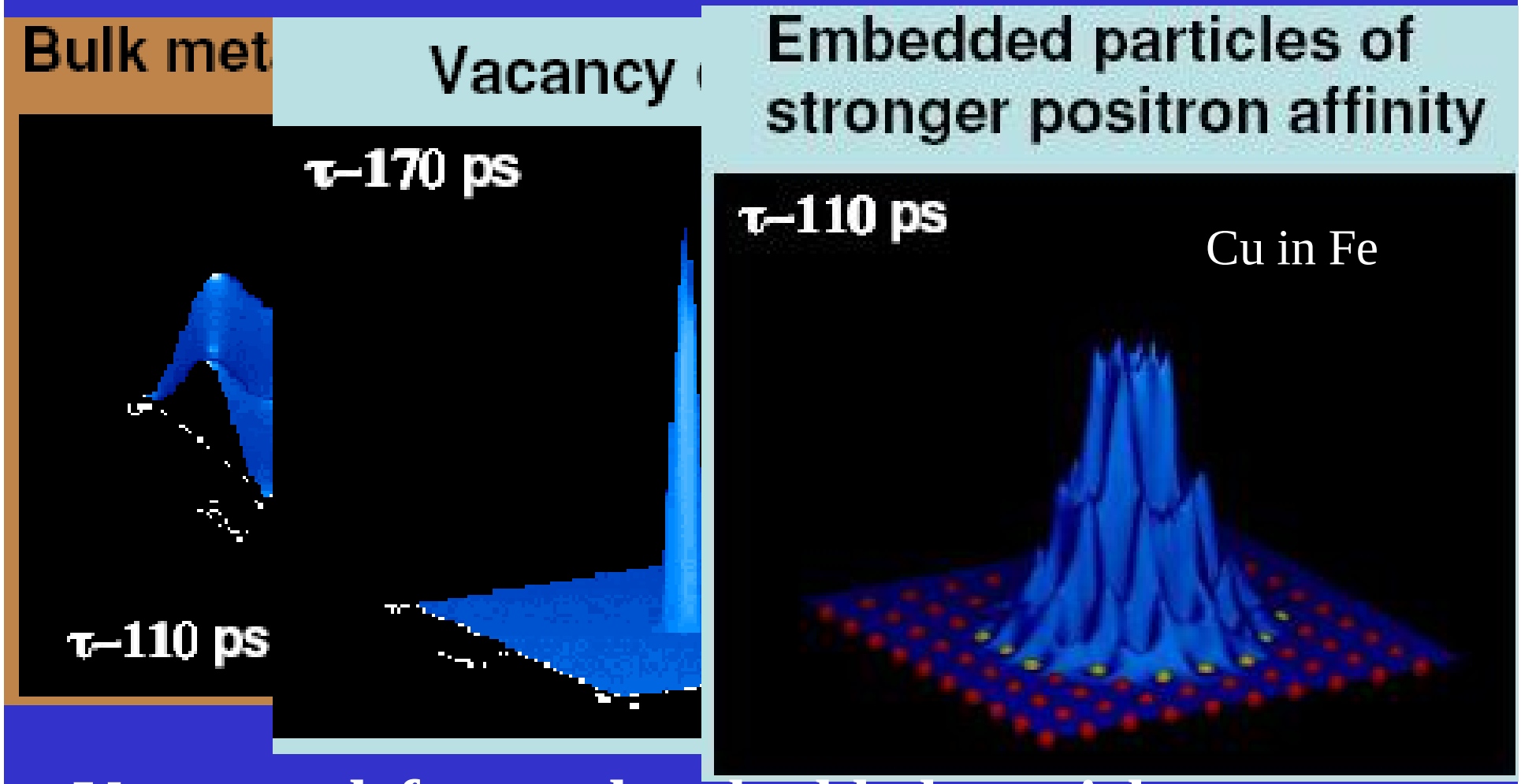

Vacancy defect and embedded particles strongly localized positron density

Irr

[1]The Oarai Br

PH

与Cu核心电子的湮没率

Fe-0.05wt%Cu, 80%

Fe-0.15wt%Cu, 92%

Fe-0.3wt%Cu, 94%

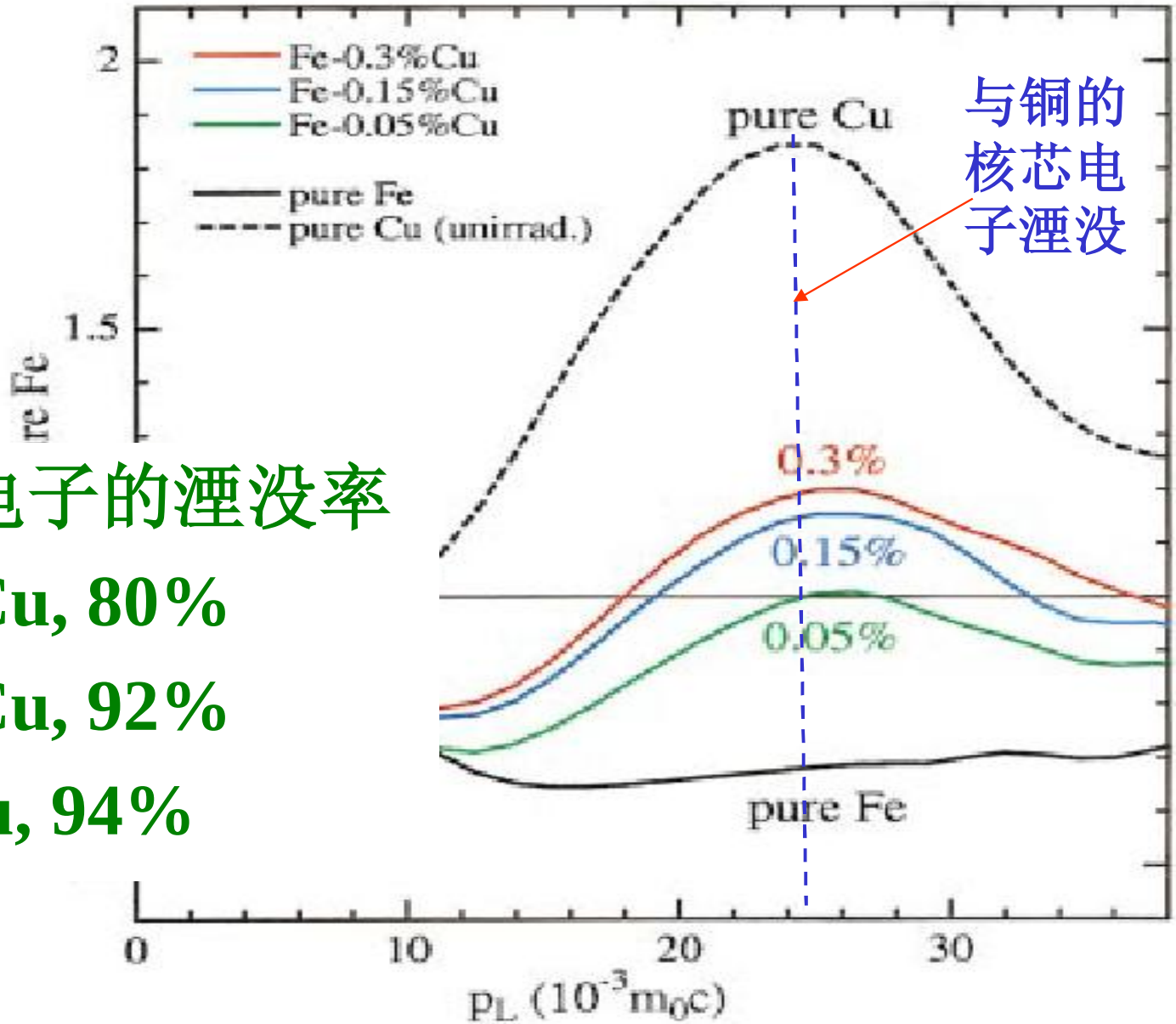

FIG. 2. (Color) CDB ratio spectra for Fe 0.3% Cu, Fe 0.15% Cu, Fe 0.05% Cu, and pure Fe irradiated with fast neutrons at about 300 °C, together with that for unirradiated pure Cu.

3. Quantum-dot

PHYSICAL REVIEW B **66**, 041305(R) (2002)

Direct observation of energy-gap scaling law in CdSe quantum dots with positrons

M. H. Weber,[1] K. G. Lynn,[1,2] B. Barbiellini,[3] P. A. Sterne,[4] and A. B. Denison[5]
[1]*Department of Physics, Washington State University, Pullman, Washington 99164-2814*
[2]*Center for Materials Research, Washington State University, Pullman, Washington 99164-2711*

实验条件

- CdSe 样品直径分别为 6 nm, 4.4 nm, 3.6 nm, 2.5 nm, and 1.8 nm, 尺寸误差约 12%.
- 样品溶解在三氯甲烷(chloroform)沉积在玻璃或抛光的硅盘上.
- 单晶 CdSe 作为参考样品.
- 单能正电子能量从1 -5 keV 取决于样品厚度.
- 99% 的正电子注入到CdSe量子点上.

The CdSe nanocrystals of different sizes exhibit different colors. With decreasing crystal size the band gap of the crystal increases and the dot gives off more energetic, or bluer photons.

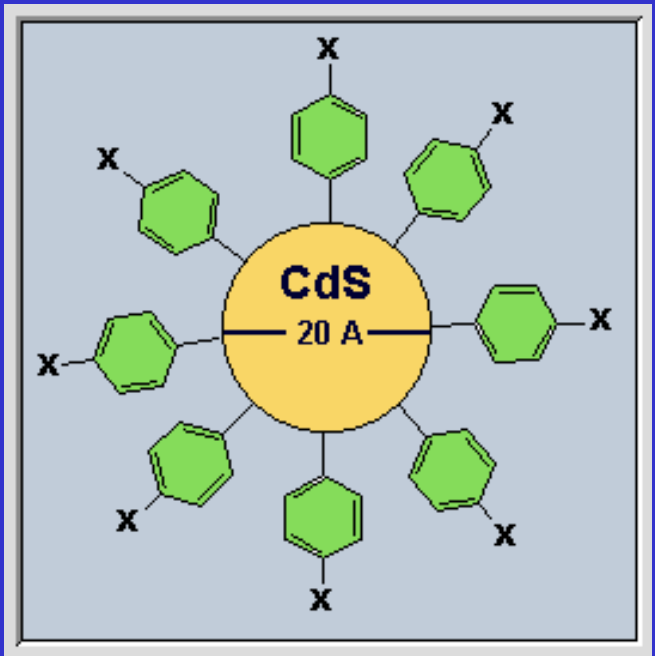

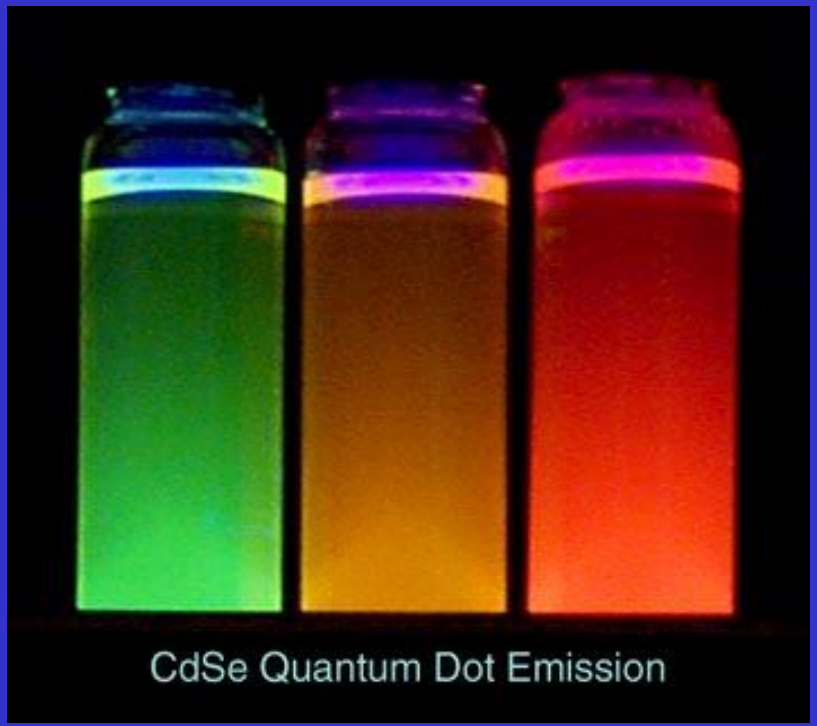

The picture shows CdSe nanocrystals of different radius r (between 1.5 nm and 3 nm) in solution. The effect of quantum confinement of electrons and holes caused by the small size of the nanocrystals can clearly be seen by the change in color.

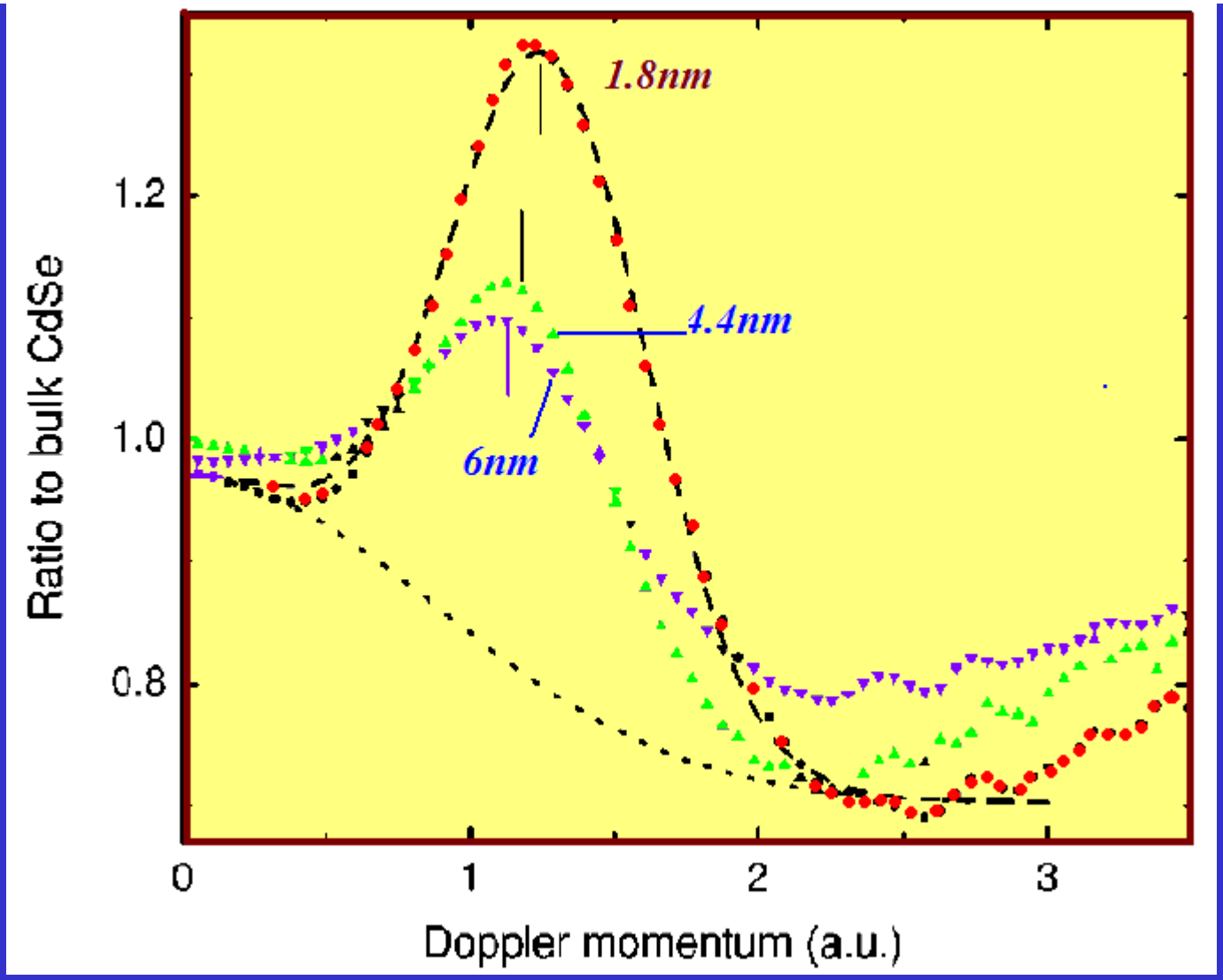

With decreasing size of the quantum dots these peaks increase in area and shift to higher momentum.

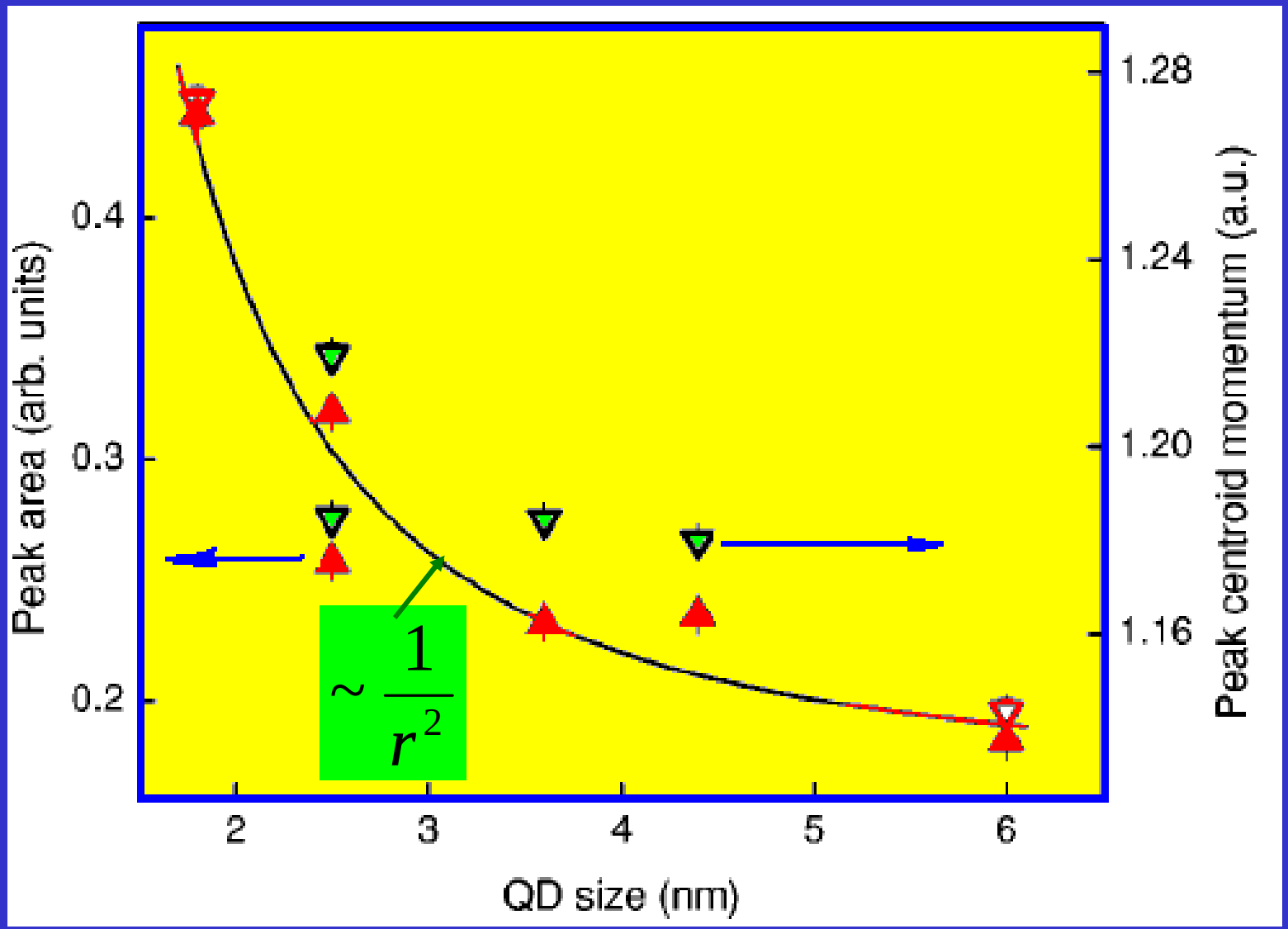

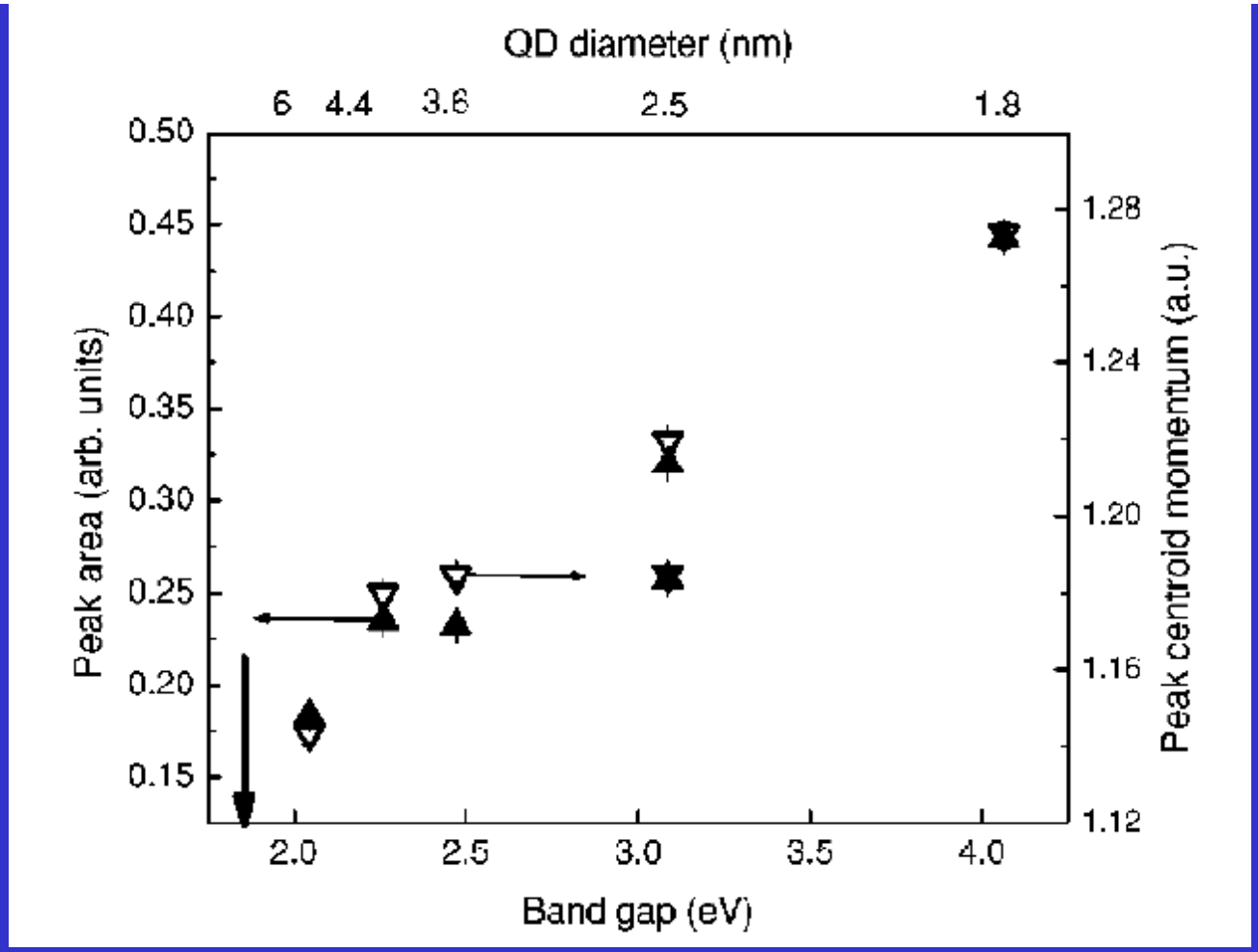

- Peak area (solid up triangles; left axis) and centroid(open down triangles; right axis) versus the band gap energy given by Wang in Ref. 18. The arrow points to the bulk crystal band-gap energy estimate as extrapolated from the size dependency.

- Moreover, the calculations for the positron affinity for CdSe, following the method in Refs. 22,23, indicate that the positron cannot escape from CdSe and its nanoparticles.
- Theoretical CdSe positron affinity (~9.0 eV) based on the LMTO calculations.
- the positron work function can be deduced as 2.38 eV. Since it is positive, thermalized positrons cannot be emitted from the CdSe surface.
- Positronium work function 2.2eV is also positive, indicating that positrons cannot be emitted from a CdSe sample either as free positrons or as positronium.

正电子寿命测量完全同意以上结论

- 用2kV能量的正电子测量块材CdSe 样品, 寿命为275 ps
- 理论计算是279 ps (GGA theory
- 6-nm CdSe 寿命测量值是 251 ps, 已接近块材寿命.
- 长寿命(>1 ns)只占1.3% 表明在CdSe内部和表面几乎没有正电子偶素形成.

4. Quantum-dot-like state

- **Positron confinement in ultrafine embedded particles: Quantum-dot-like state in an Fe-Cu alloy**
- Y. Nagai
- *The Oarai Branch, Institute for Materials Research, Tohoku University, Oarai, Ibaraki 311-1313, Japan*
- *PRB2000*

5. Quantum antidots

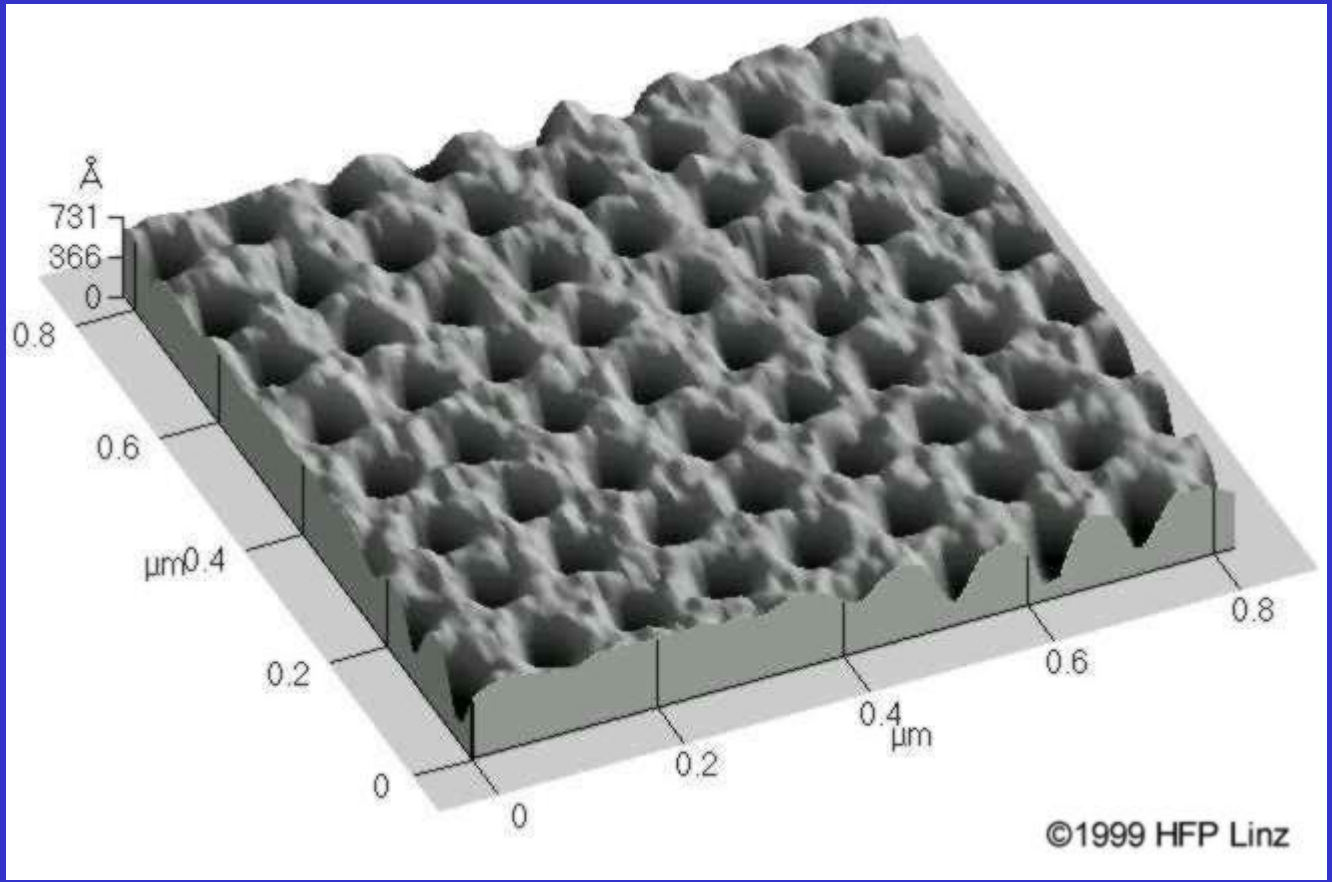

Thin magnetic films (10 nm) with periodic holes

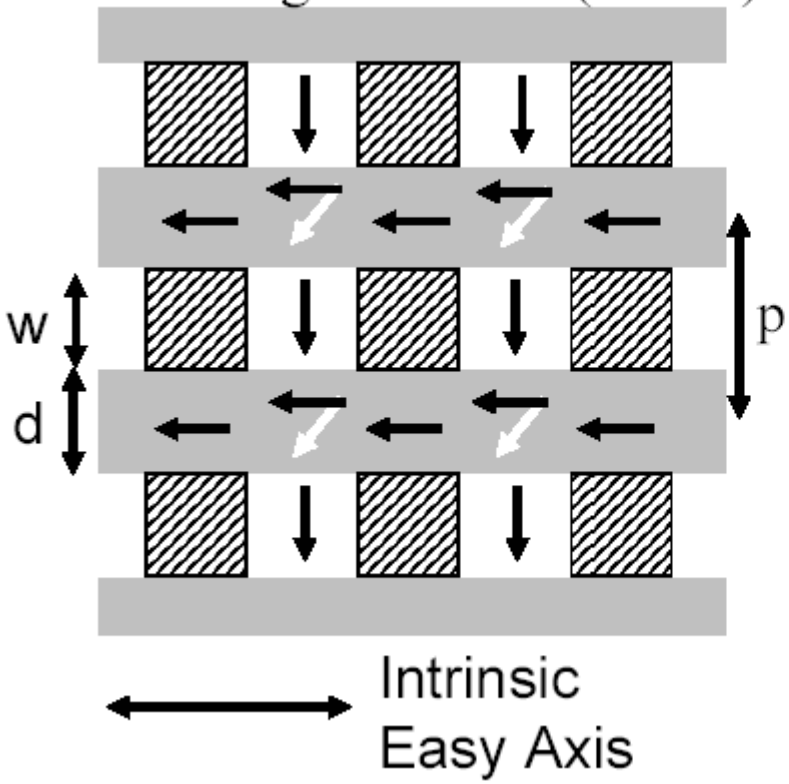

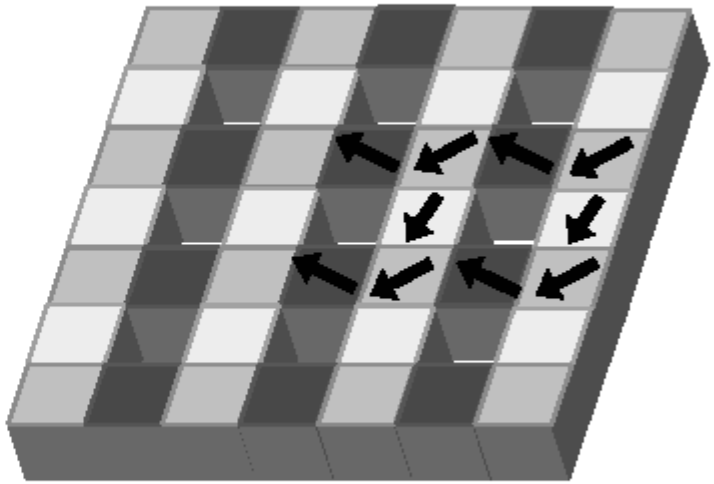

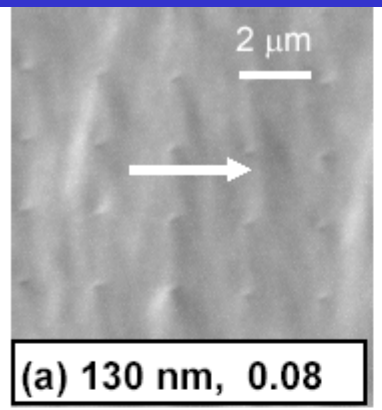

Intrinsic Easy Axis

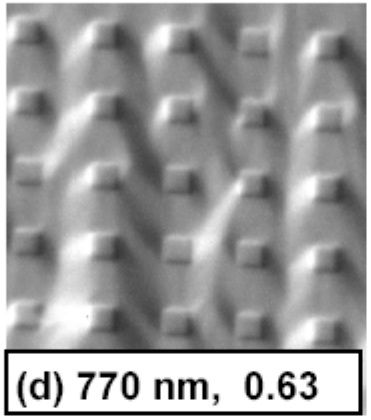

Magnetization Sensitivity

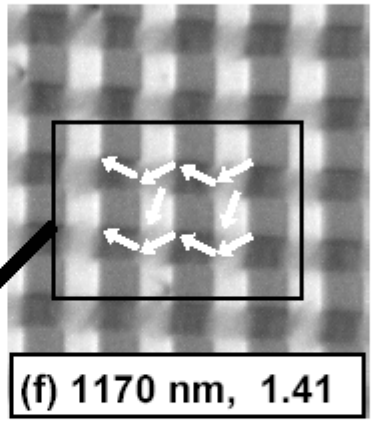

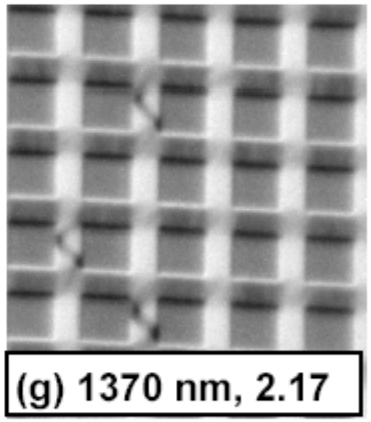

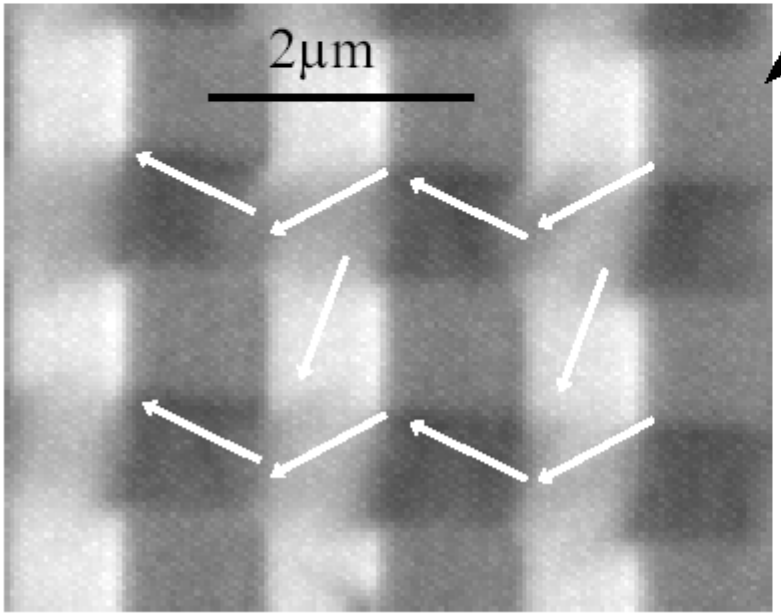

In good agreement with micromagnetics

L. Lopez-Diaz et al. J. M. M. Mater. (1999)
L. Torres et al. Appl. Phys. Lett. (1998)

Vacancy Defects on Surfaces of Au Nano-particles Embedded in MgO
*PRL, **83** (1999) 4856, Jun Xu(Oak Ridge)*

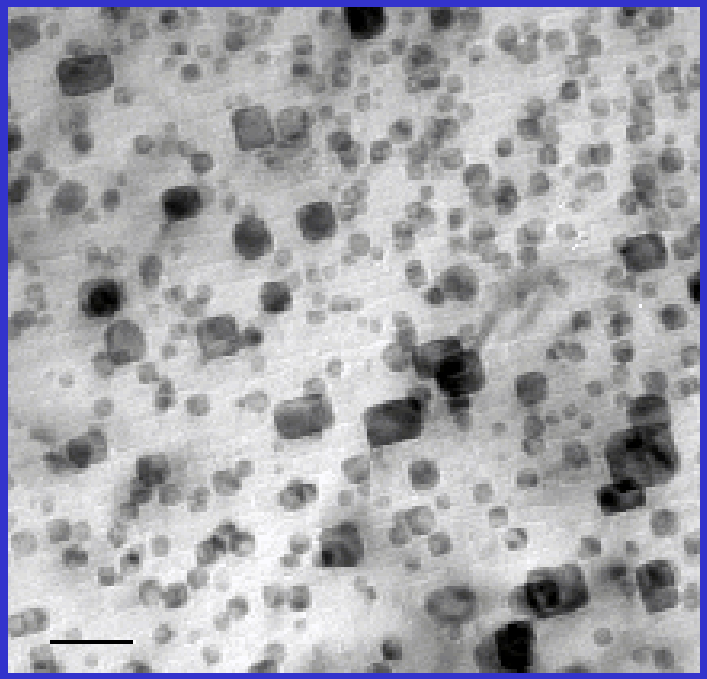

TEM of Au Nano-particles in MgO

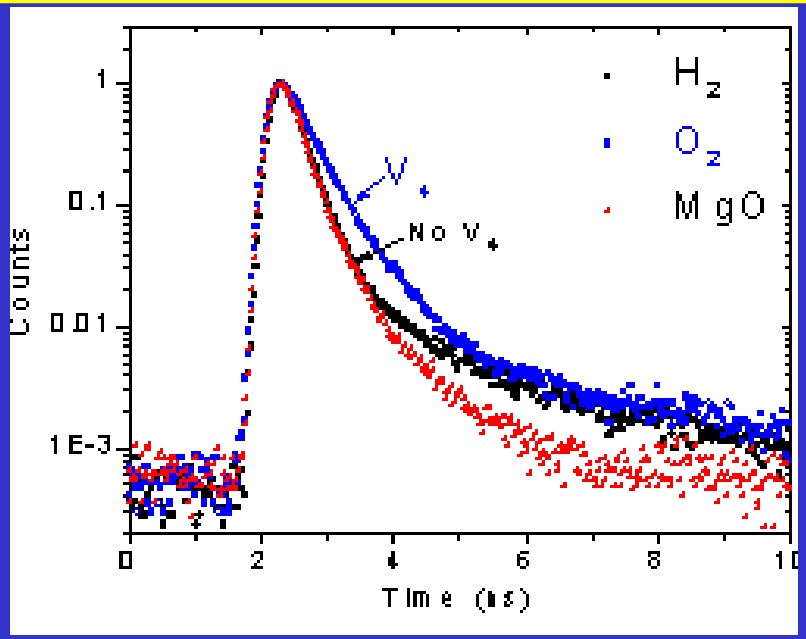

Positron lifetime spectra for MgO and embedded Au nanoparticle layers generated by annealing in O_2 or H_2, respectively

样品制备

- MgO(100)
- Au 1.1MeV, 1,3,6 and 10×10^{16}Au ions/cm^2,
- Au ions range 0.16-0.4μm.
- Annealing 1200ºC in Ar+5%O_2.

正电子湮灭位置

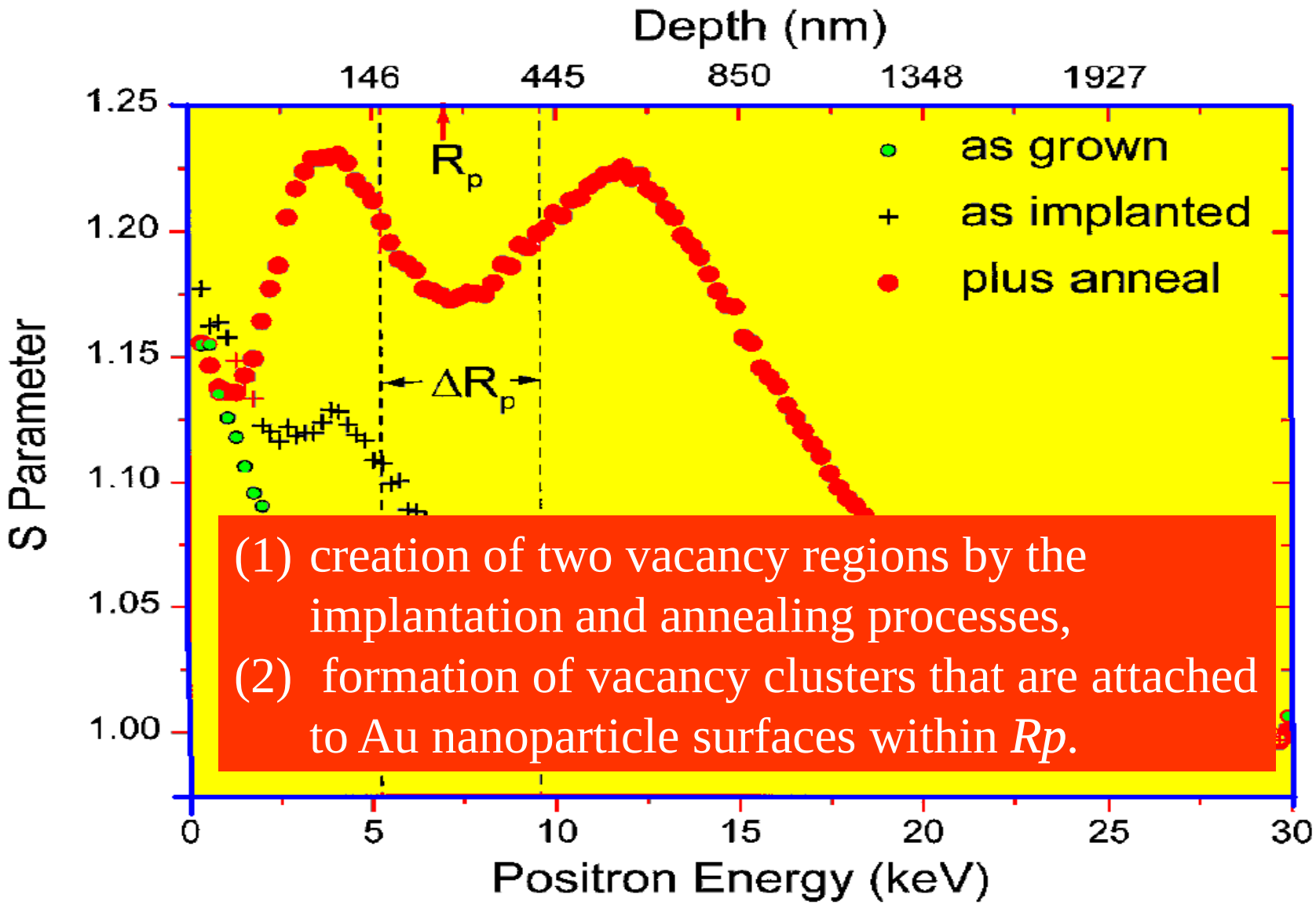

(1) creation of two vacancy regions by the implantation and annealing processes,

(2) formation of vacancy clusters that are attached to Au nanoparticle surfaces within *Rp*.

1200ºC 90min annealed in Ar+5%O_2.

1.1MeV, 6×10^6ions/cm^2.

缺陷的类型

- Positron lifetime spectra were measured at two mean depths:
- ~0.15 μm(23KeV) centered in the Au implantation layer;
- ~1.7 μm(5KeV) that was deep into MgO layer where Au implantation is believed to least affect.

~1.7 μm	220ps±40ps (89%±3%)	590ps±70ps (11%±3%)
~0.15 μm	320ps±50ps (95%)	1.32ns±0.3ns (5%)

PRB.64, 113404, 2001
Jun Xu et al.

- Positron lifetime spectra were measured at two mean depths:

MgO, 210ps

- ~0.15 μm centered in the Au implantation layer;
- ~1.7 μm that was deep into MgO layer where Au implantation is believed to least affect.

~1.7 mm	220ps±40ps (89%±3%)	590ps±70ps (11%±3%)
~0.15 mm	320ps±50ps (95%)	1.32ns±0.11ns (5%)
~0.15 mm Annealing	410ps±80ps (90%)	1.8ns±0.3ns (7%)

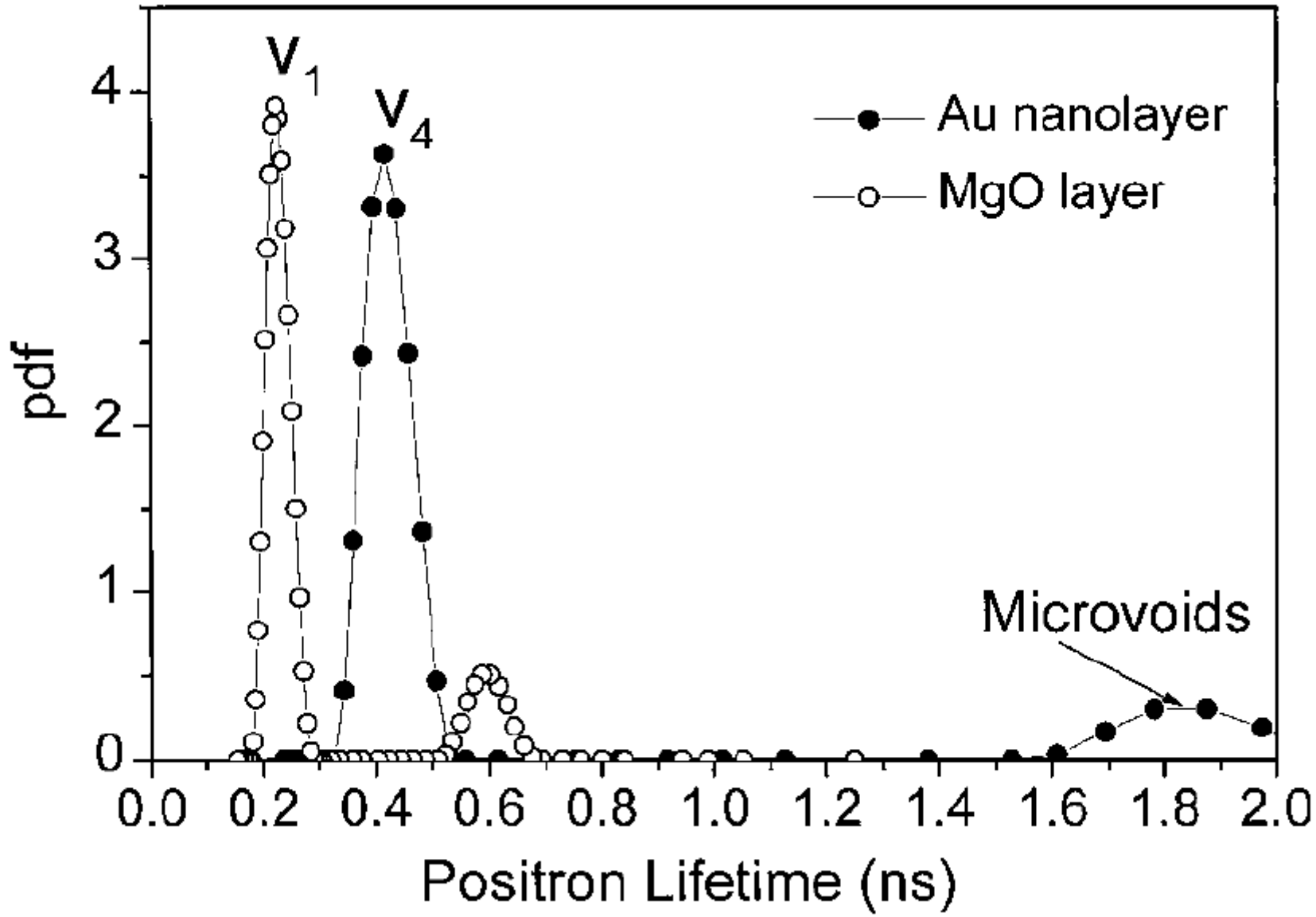

Positron lifetimes of MgO

Defect site	Calculated position lifetime (ps)	Measured positron lifetime (ps)
Perfect MgO	155	160 (Ref. 13)
V_O	157	
V_{Mg}	244	210 (Ref. 14)
$V_{Mg}-V_O$	290	
$V_{Mg}-V_{2O}$ (triangle)	338	300–340
$V_{Mg}-V_{2O}$ (linear)	329	
$V_{2Mg}-V_O$ (triangle)	330	
$V_{2Mg}-V_O$ (linear)	310	
$V_{2Mg}-V_{2O}$	414	375–400

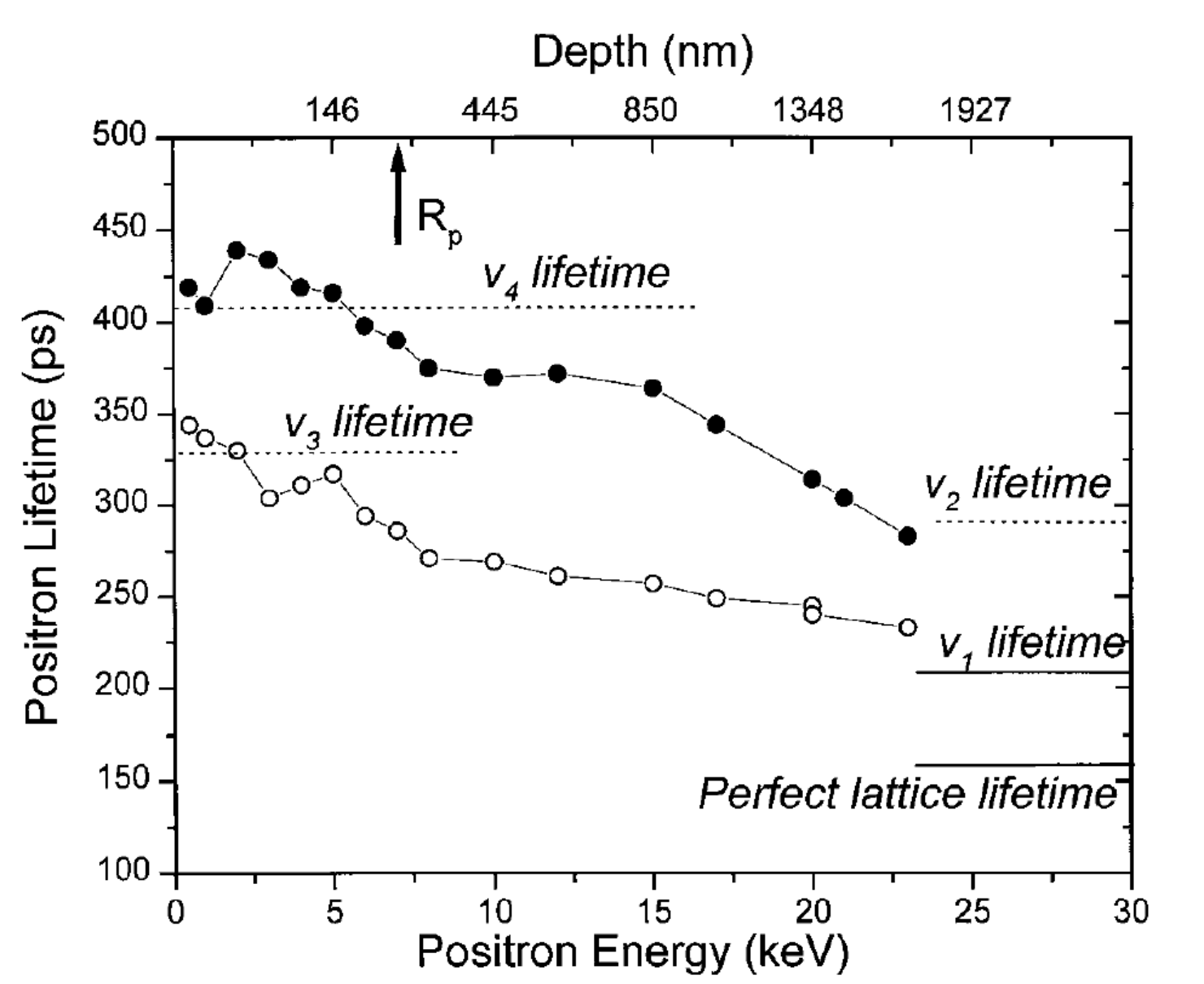

- V3,V4 lifetimes vs. positron energy

与剂量的关系

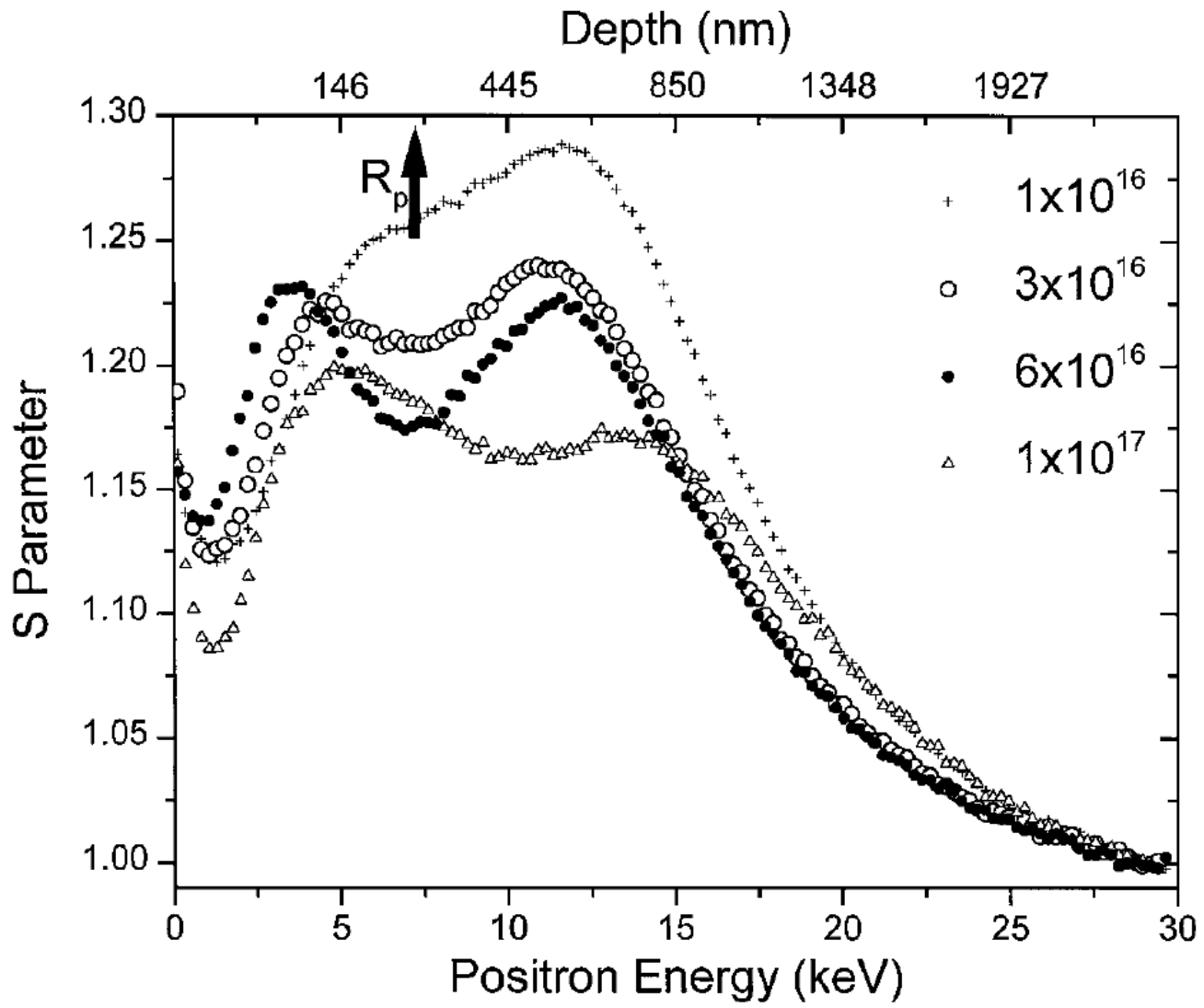

Au-V4 complexes

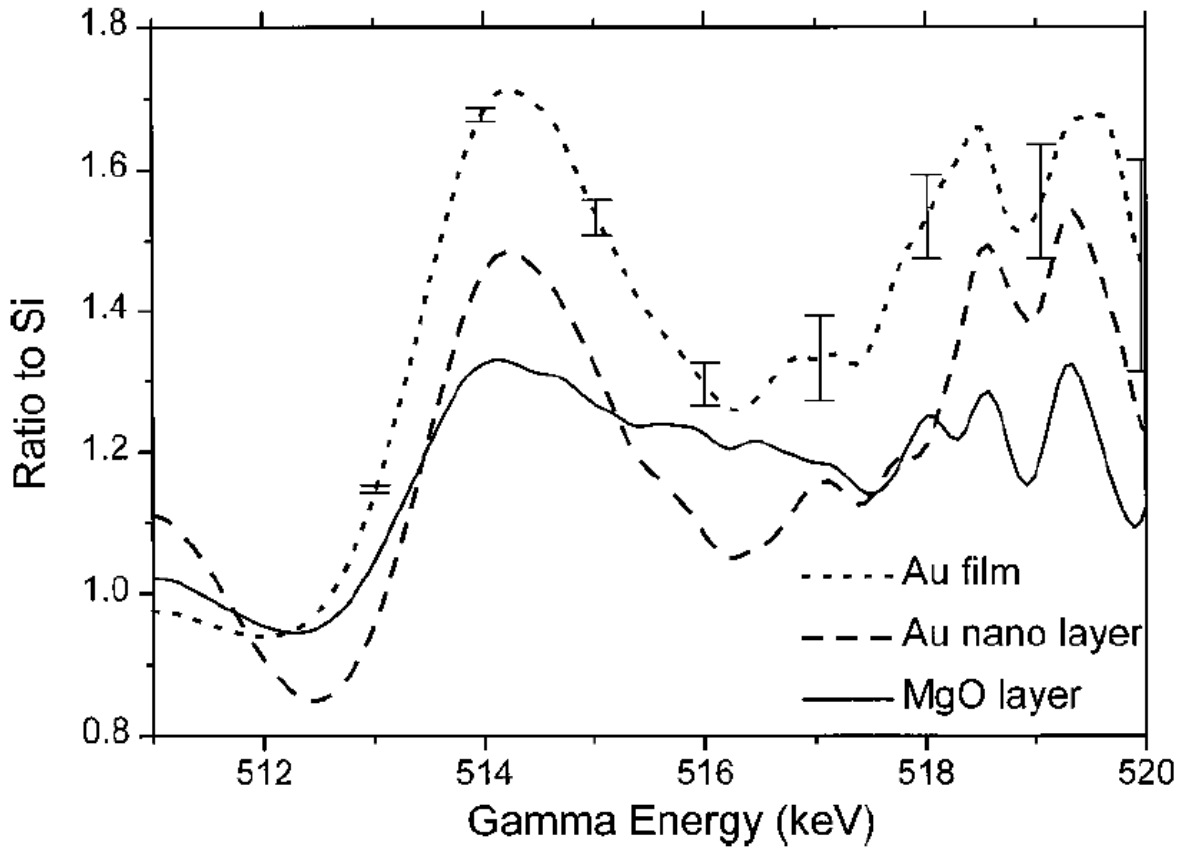

- positrons, trapped at the v_4 sites annihilate with the electrons associated with Au nanoparticles. Of course, the defects' environment also includes the MgO matrix which also contributes to the energy spectrum. This shows that the vacancy sites, where the positrons are trapped, are located in the interface between Au nanoparticles and the MgO matrix.

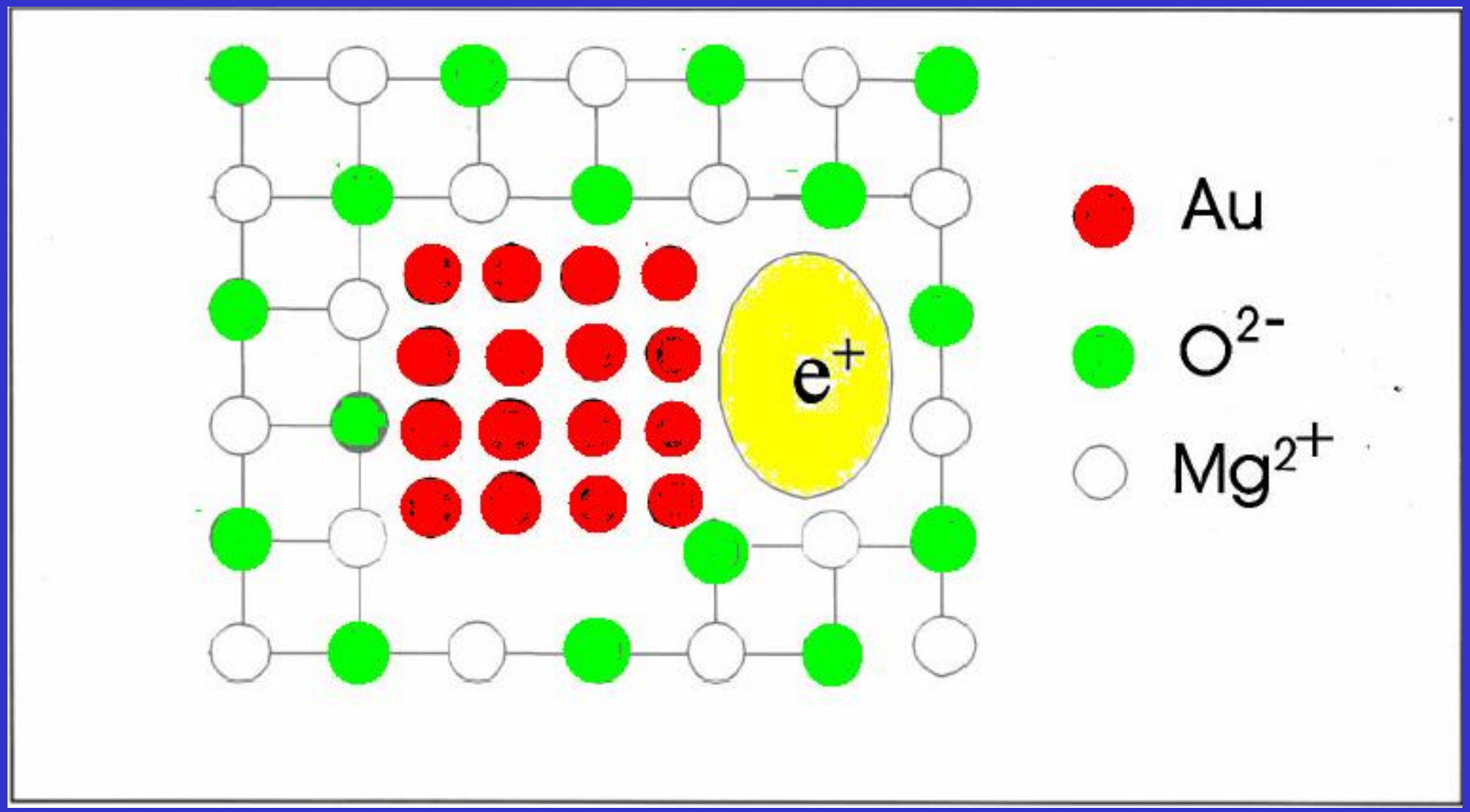

The electrons of Au atoms that are next to the clusters annihilate with the trapped positrons, resulting in annihilation momentum structure of the Au atoms.

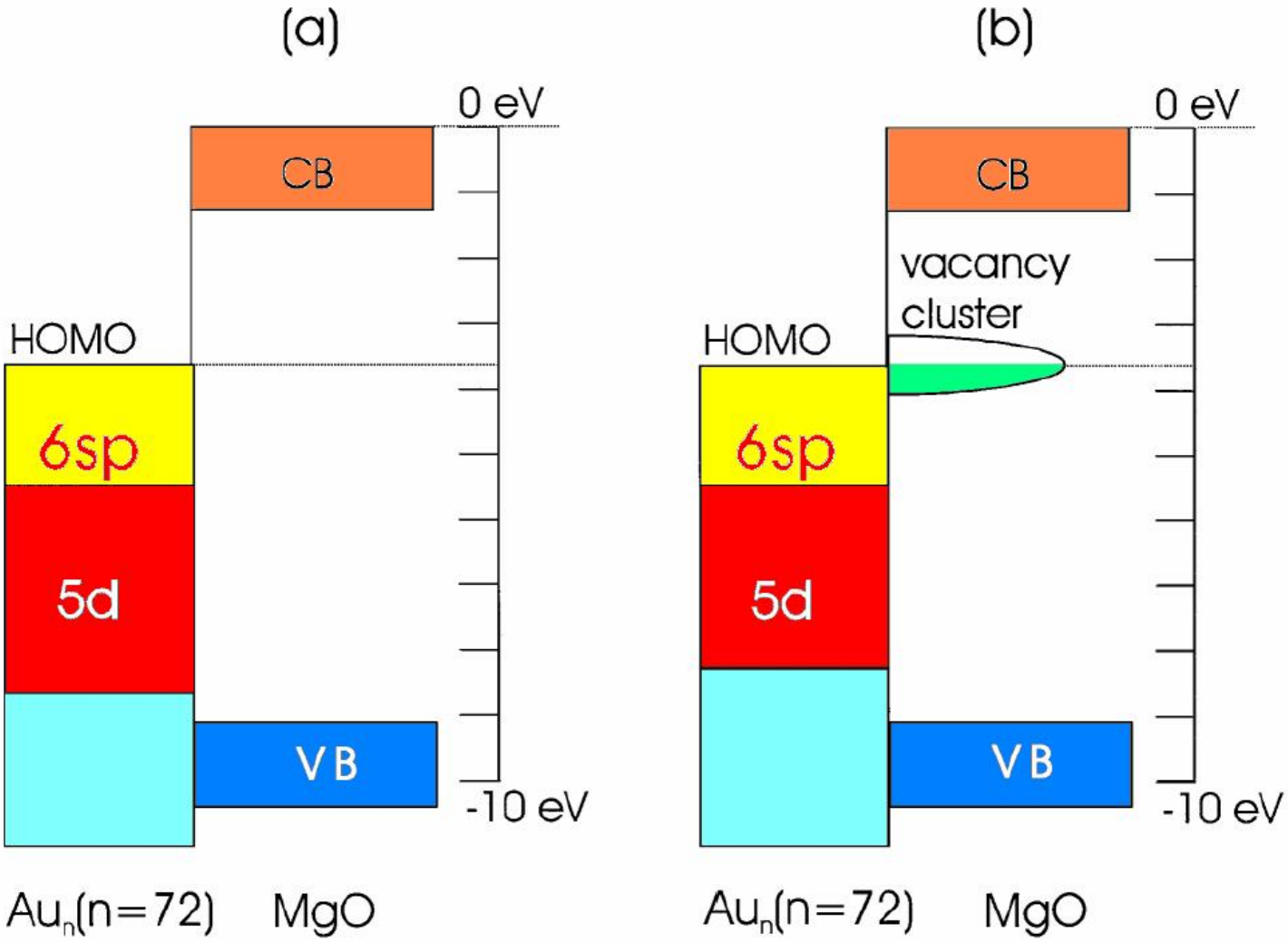

FIG. 3. Schematic diagrams of the energy band structure for the interface between Au nanoparticles and solid MgO. (a) Au nanoparticle with no surface defects. (b) Au nanoparticle with a surface vacancy cluster.

O_2可以,H_2不能形成Au-V4 complexes

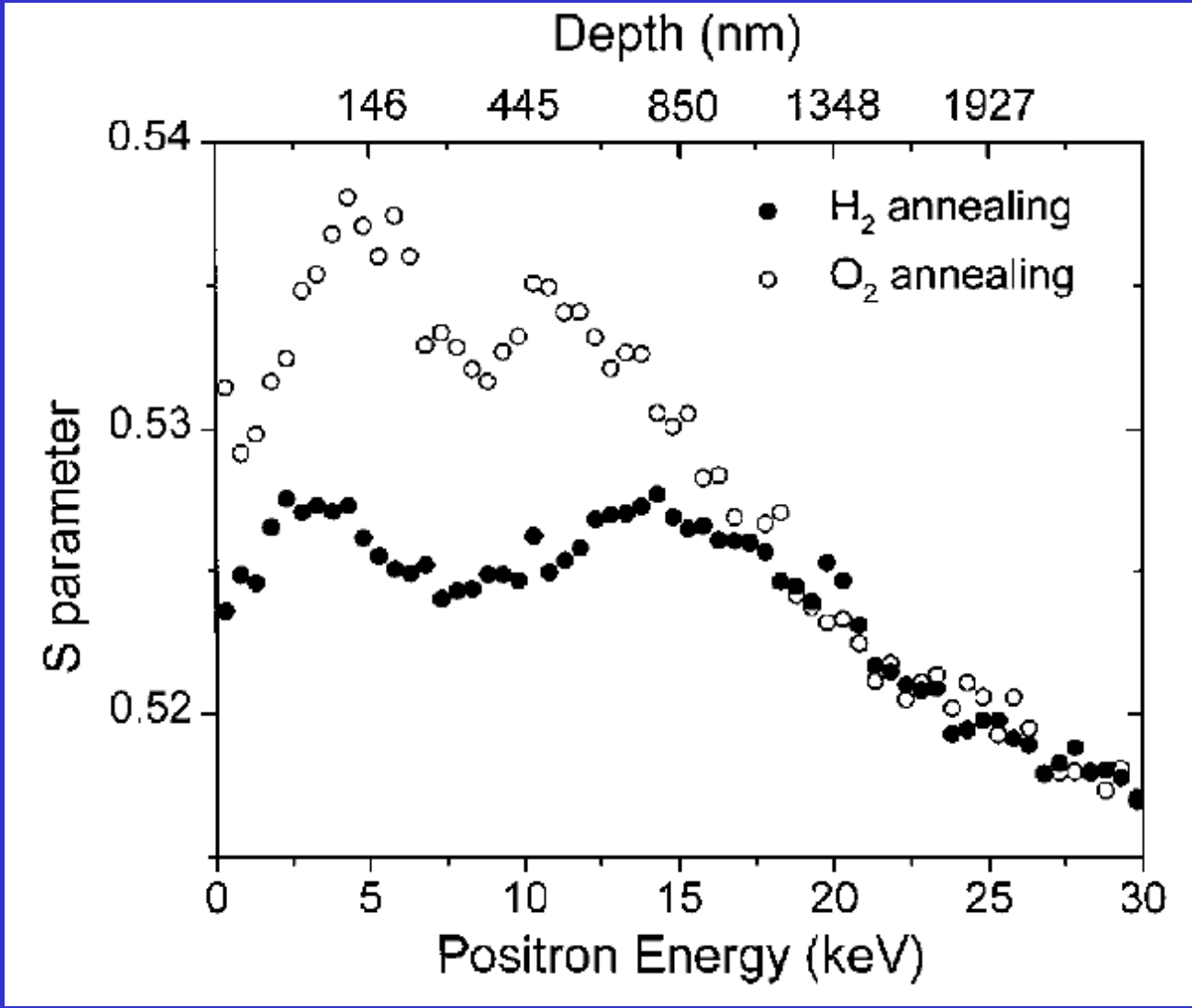

- Nanoparticles prepared by annealing in O_2 show a longer lived state labeled v_4. This state is associated with clusters of four atomic vacancies located on the surface of the Au particles. The surface vacancy clusters are not seen on the nanoparticles prepared in H_2.
- The v4 clusters are related to the "red" shift in the following way: for Au nanoparticles generated in O_2, electrons are transferred from the Au nanoparticles to the interface vacancy clusters, resulting in a reduced electron density on the nanoparticles, therefore the frequency decreases.

能否观测到Au-V_4

Direct imaging of quantum antidots in MgO dispersed with Au nanoclusters

C. M. Wang

Pacific Northwest National Laboratory, P.O. Box 999, Richland, Washington 99352

APPLIED PHYSICS LETTERS **87**, 153104 2005

Sample

- Au^{2+}, 2MeV at 975K implanted MgO
- Implan rmal.
- Anneal
- Ion flu

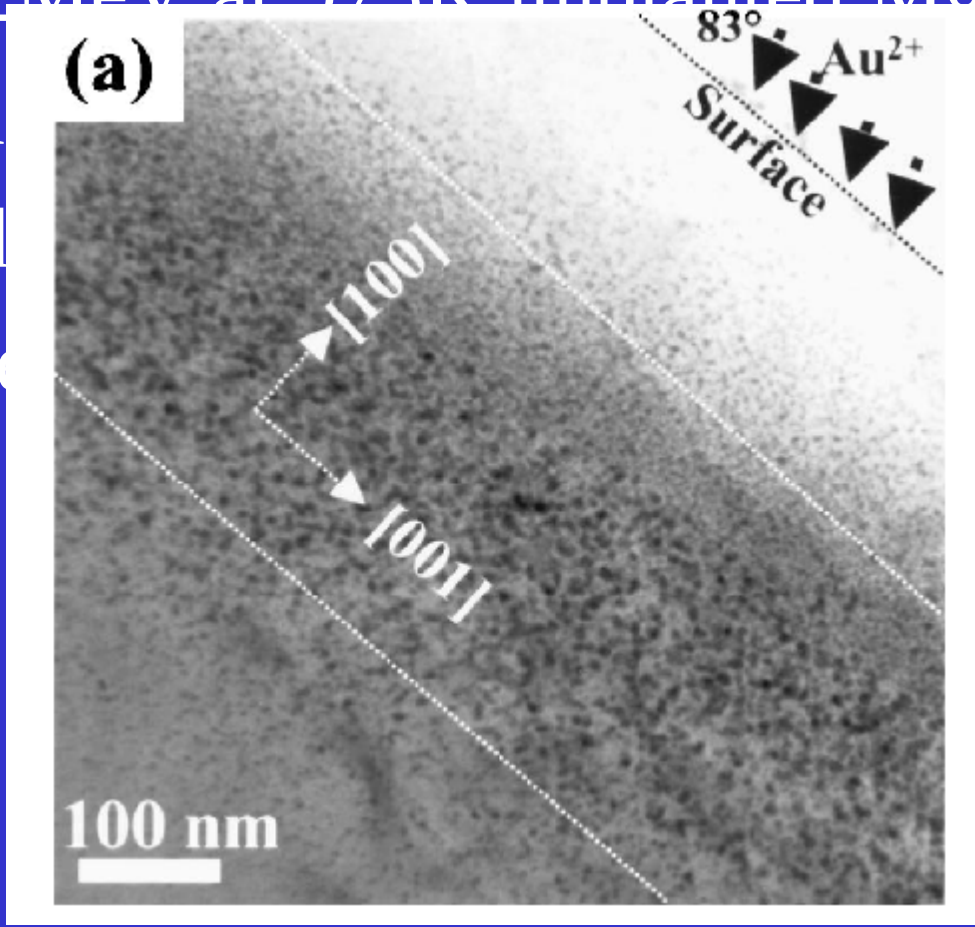

Microscopy

- high-resolution transmission electron microscopy(HRTEM)
- high-angle annular dark-field imaging HAADF in aberration-corrected scanning transmission electron microscopy STEM.(HAADF-STEM).
- HAADF, 100KV, probe size 0.13nm, 50pA

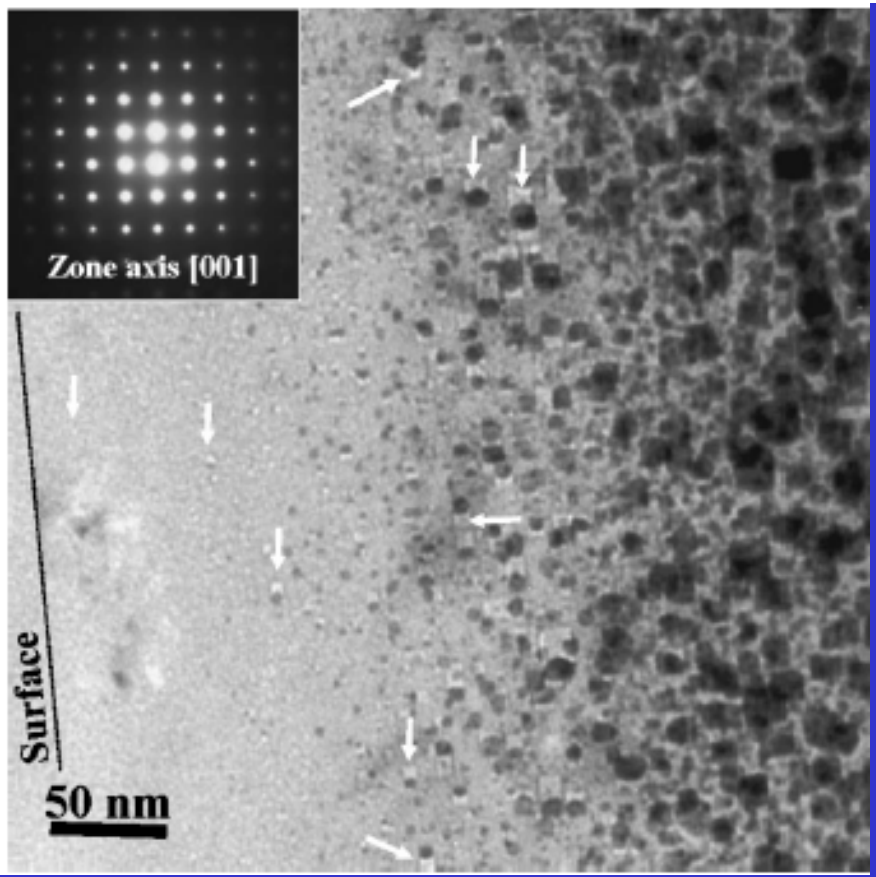

Au clusters having a diameter of 6.5 nm.

Cross-sectional TEM image showing the general microstructural features of the Au implanted MgO. The inset is the selected area electron diffraction pattern. The white areas indicated by the white arrows are vacancy clusters as revealed by the HAADF-STEM imaging.

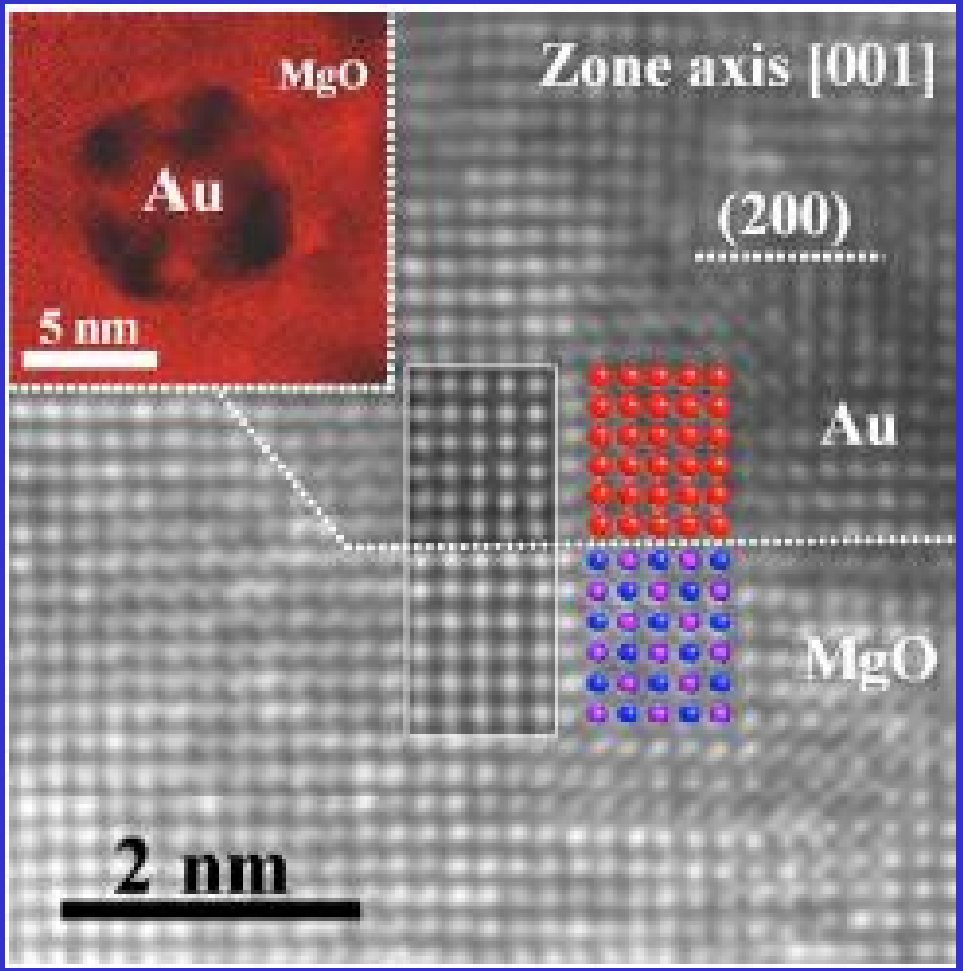

MgO{100 }//Au{100 } interface,

HRTEM image showing interface between Au cluster and MgO. The inset at the top is a representative HRTEM image showing a faceted Au cluster and the insets in the middle are the proposed atomic structural model and the calculated HRTEM image.

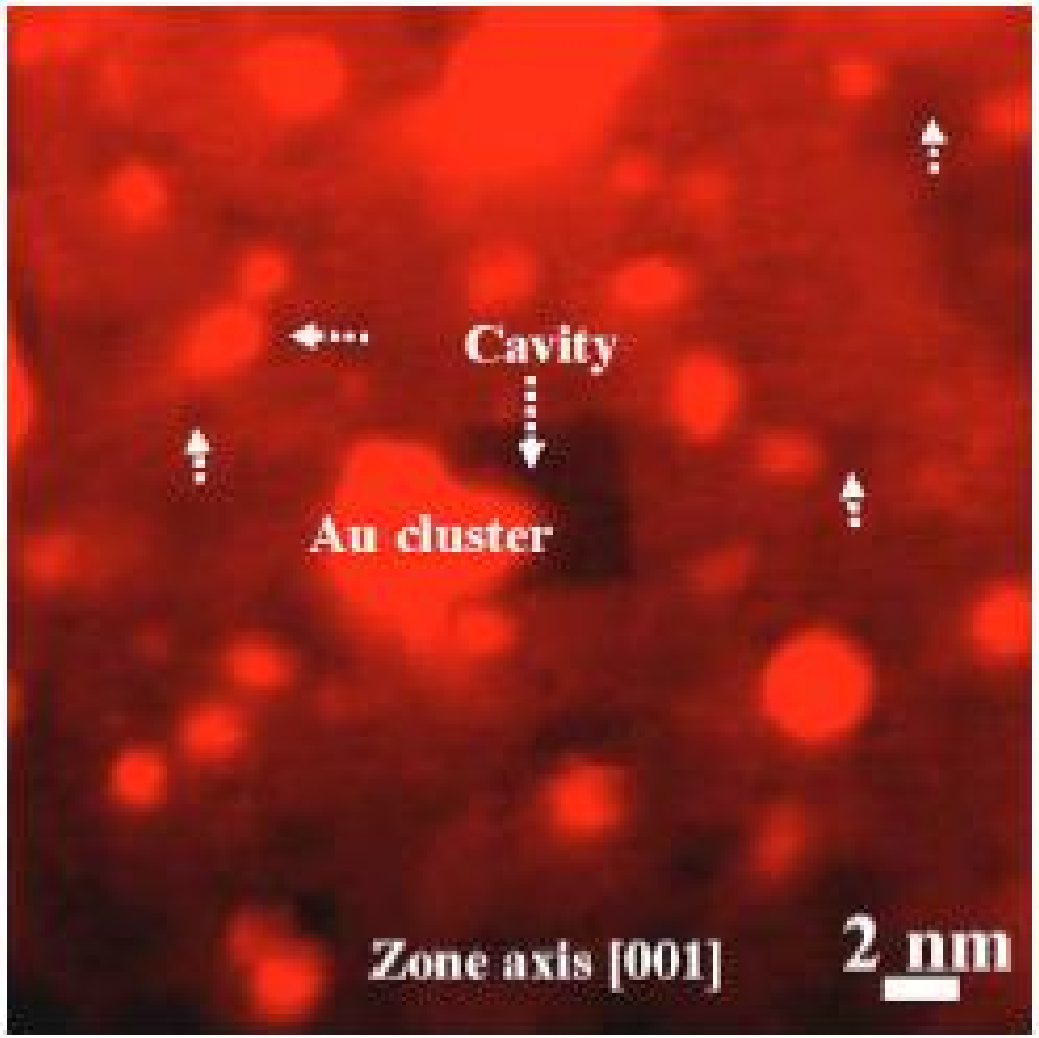

Two sources of vacancies can be considered:

- Thermally excited vacancies;
- Au bombardment induced vacancies.

HAADF-STEM image showing high concentration of Au clusters mixed with faceted cavities vacancy clusters are marked by the arrows.

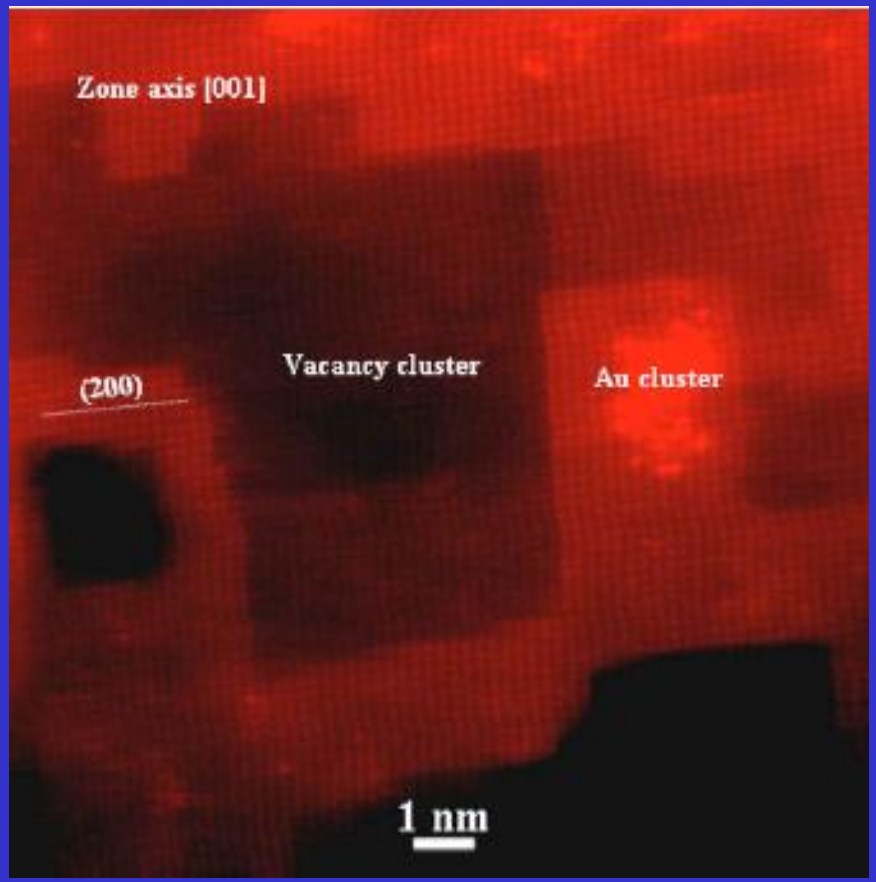

HAADF-STEM image taken from Au clusters dilutely distributed regions in Fig. 1. The dark contrasted regions are the vacancy clusters. Note the faceting of the vacancy cluster at the 001 planes as well as the thickness change along the electron beam direction.

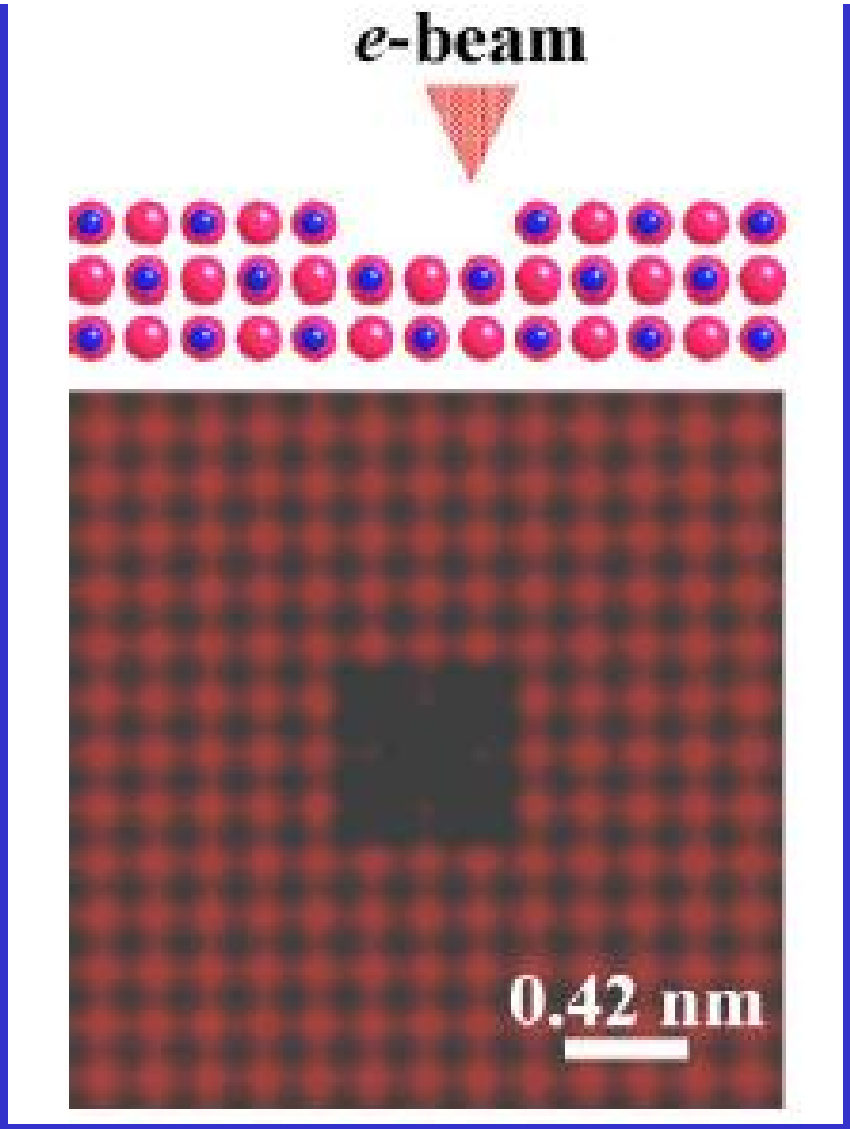

Atomic structural model with vacancy cluster in the center and the correspondingly simulated HAADF-STEM image.

Nanoclusters by implantation

Nanocavity formation processes in MgO(100) by light ion (D, He, Li) and heavy ion (Kr, Cu, Au) implantation

A. van Veen [a,*], M.A. van Huis [a], A.V. Fedorov [a], H. Schut [a], F. Labohm [a], B.J. Kooi [b], J.Th.M. De Hosson [b]

[a] *Interfaculty Reactor Institute, Delft University of Technology, Mekelweg 15, NL-2629 JB Delft, The Netherlands*
[b] *Department of Applied Physics, Materials Science Centre, University of Groningen, Nijenborgh 4, NL-4797 AG Groningen, The Netherlands*

Nuclear Instruments and Methods in Physics Research B 191 (2002) 610–615

MgO(1 0 0) ion implanted samples; implantation data and defect observations

Implantation				TRIM results					Nanocavities		
Ion	E_{ion} (keV)	Dose (1E16 cm^{-2})	T_{impl} (K)	R_p (ΔR_p)/ nm	Displ. (vac/ion)	Conc. (MgO fraction)	Damage displacement per MgO (dpa)		T_{anneal} (K)	Location of cavity zones (nm)	
							Surface	Maximum near R_p		PBA	XTEM
Au	30	3	1273	14 (3)	170	0.841	11.2	16.8	–	[a]	10
Au	30	1	RT	14 (3)	170	0.281	3.7	5.6	1373	[a]	10
Au	1000	1	RT	160 (31)	3300	0.022	5.6	18.7	1273	25–175 280–450	
									1473	[b]	–

[a] Depth too small for PBA observation.
[b] Voids dissolved at this temperature.

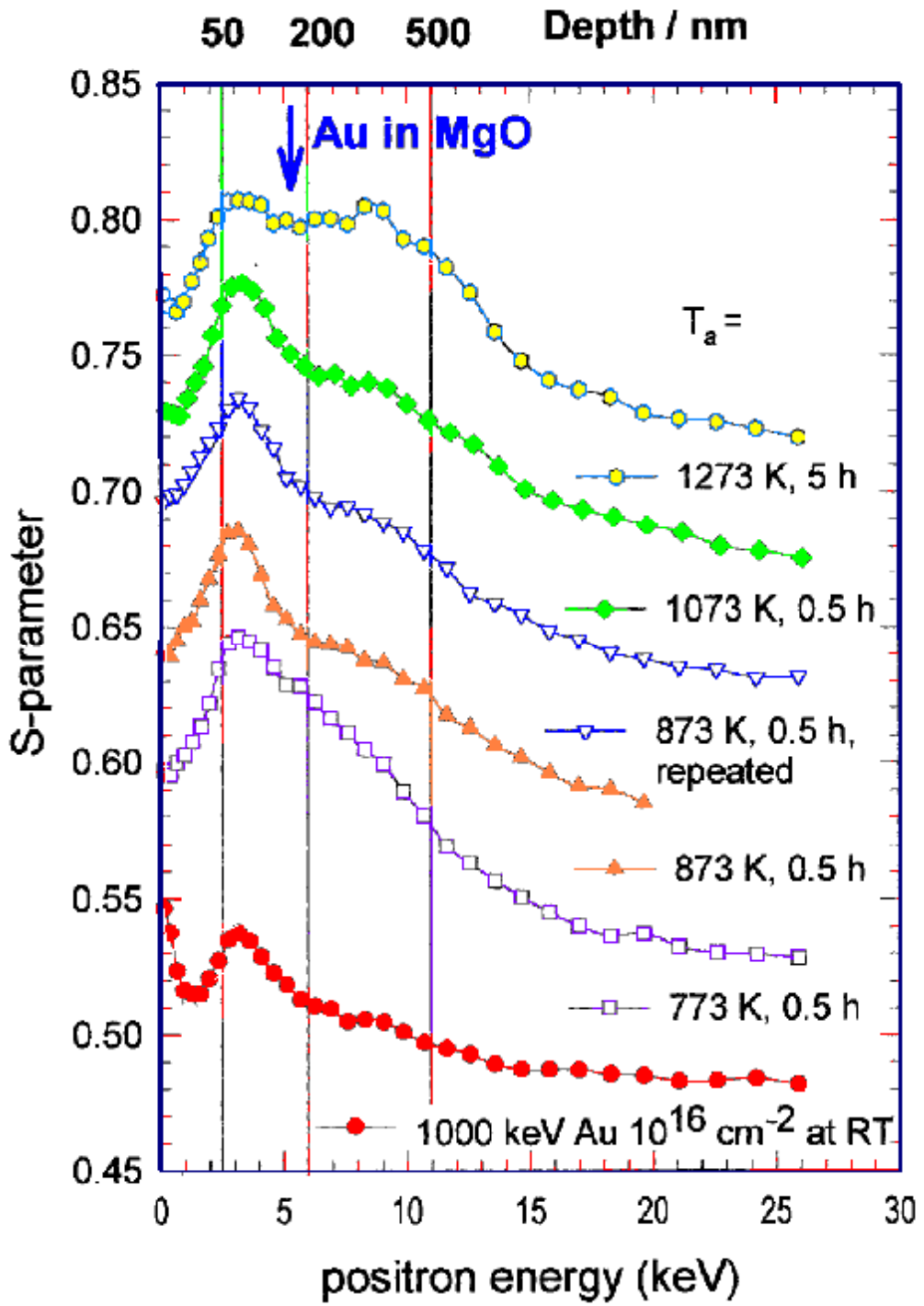

considerable increase of S
h range from 20 to 500
clustering has occurred.

opment is seen of a depth
o peaks. The valley
cated at the position of the

s in MgO dissolve so that
ates was observed.

Au with cavities - 30 keV, 10^{16} Au^{+} cm^{-2} implanted at 1273K

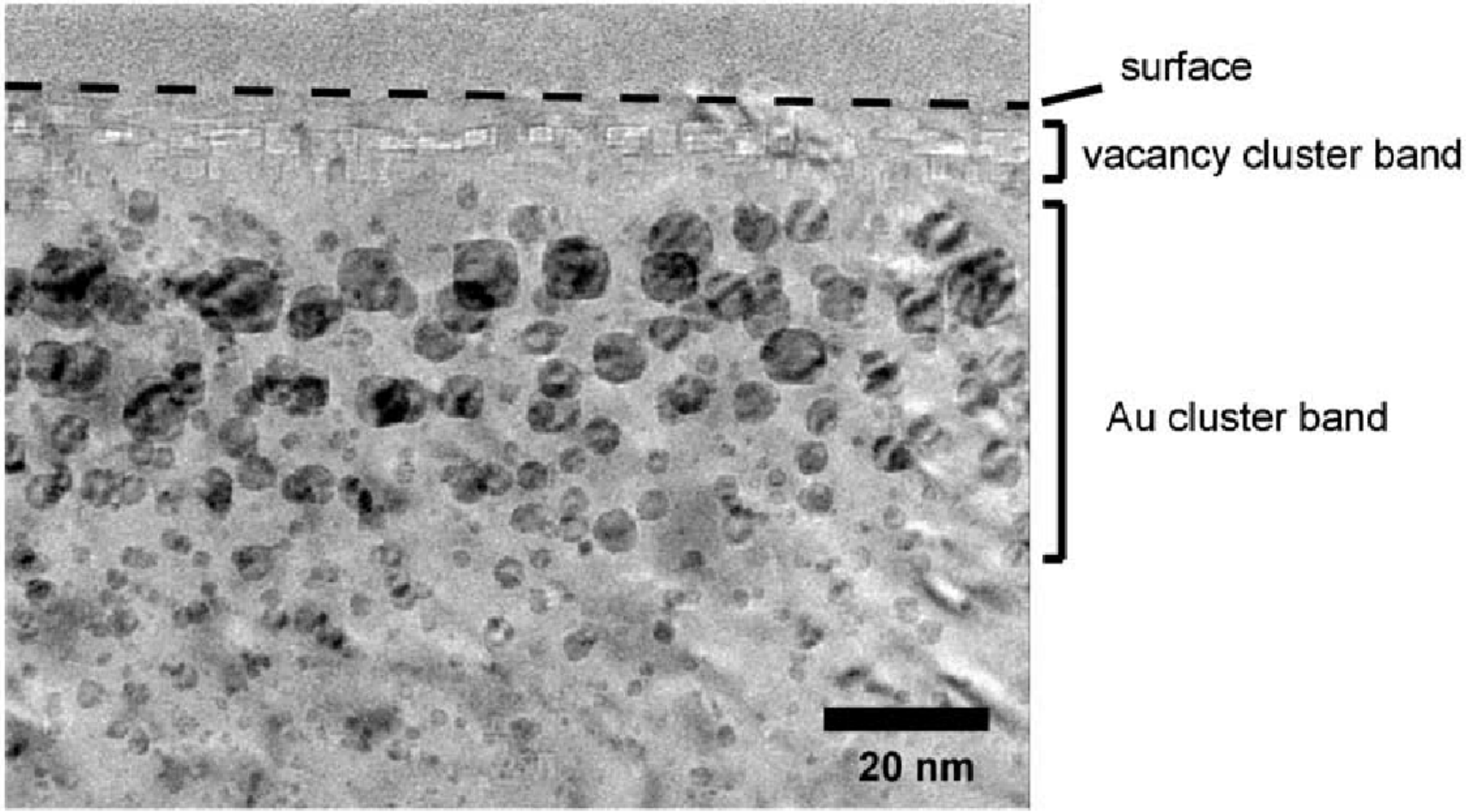

(a)

PHYSICAL REVIEW B **67**, 235409 (2003)

Formation of solid Kr nanoclusters in MgO

M. A. van Huis, A. van Veen, and H. Schut
Interfaculty Reactor Institute, Delft University of Technology, Mekelweg 15, NL 2629 JB Delft, The Netherlands

TABLE I. Sample treatment and main experimental observations.

	Sample treatment
Ion implantation	3×10^{16} Kr ions cm^{-2} at an energy of 280 keV.
Thermal anneal	At 900 K and 1100 K for a period of 30 min.
	Results
Optical absorption	*F* and *V* centers present after implantation; dissociation after 900 K anneal.
XTEM	Cubical, solid Kr clusters at 70–130 nm depth, cluster size 2–4 nm. Cubical nanovoids at 15–30 nm depth, cluster size 2–5 nm.
PBA	Defect agglomeration during annealing. High *S* parameter in nanovoids layer; *S* parameter in Kr cluster layer higher than that of bulk MgO and lower than the *S* parameter of MgO with defects.

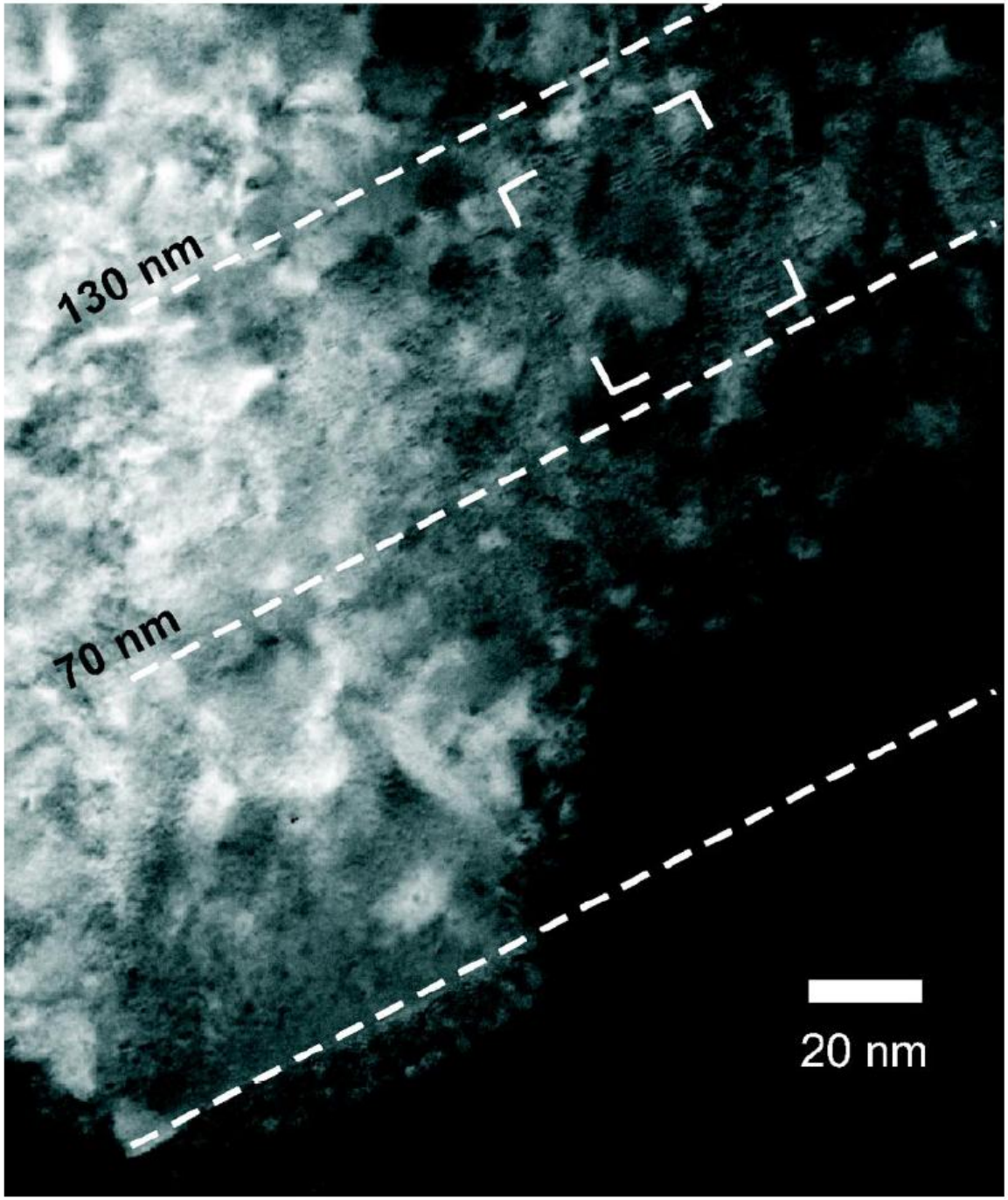

TEM overview image of Kr-implanted MgO. Solid Kr nanoclusters are observed in a band at a depth of 70–130 nm.

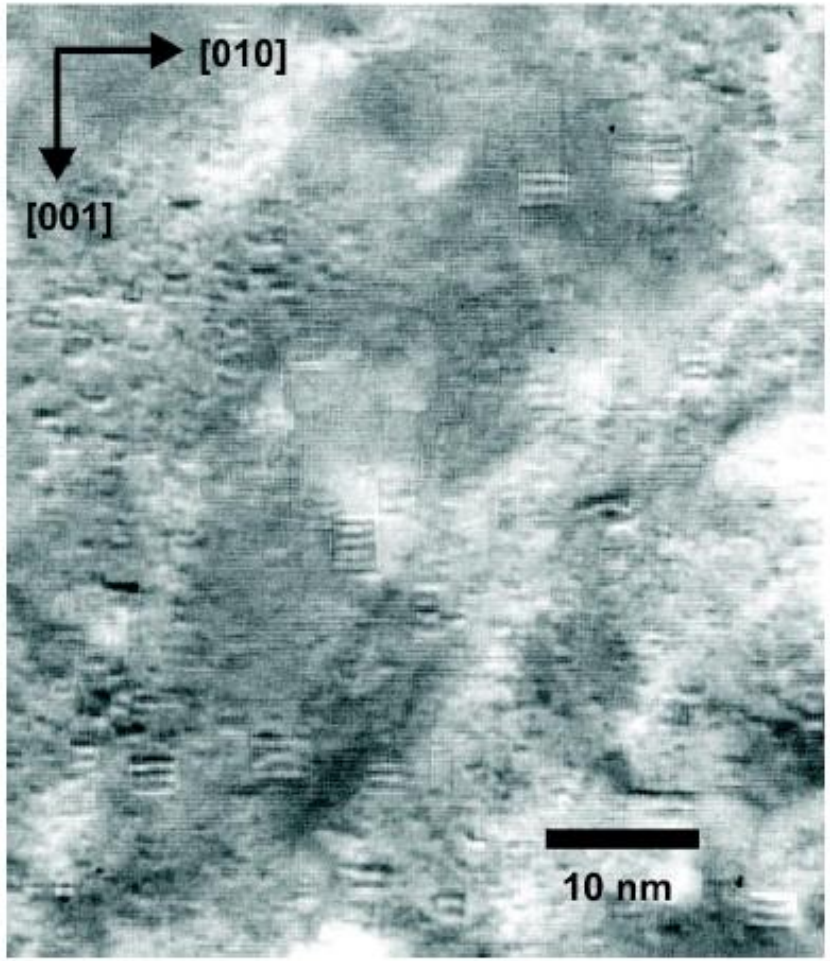

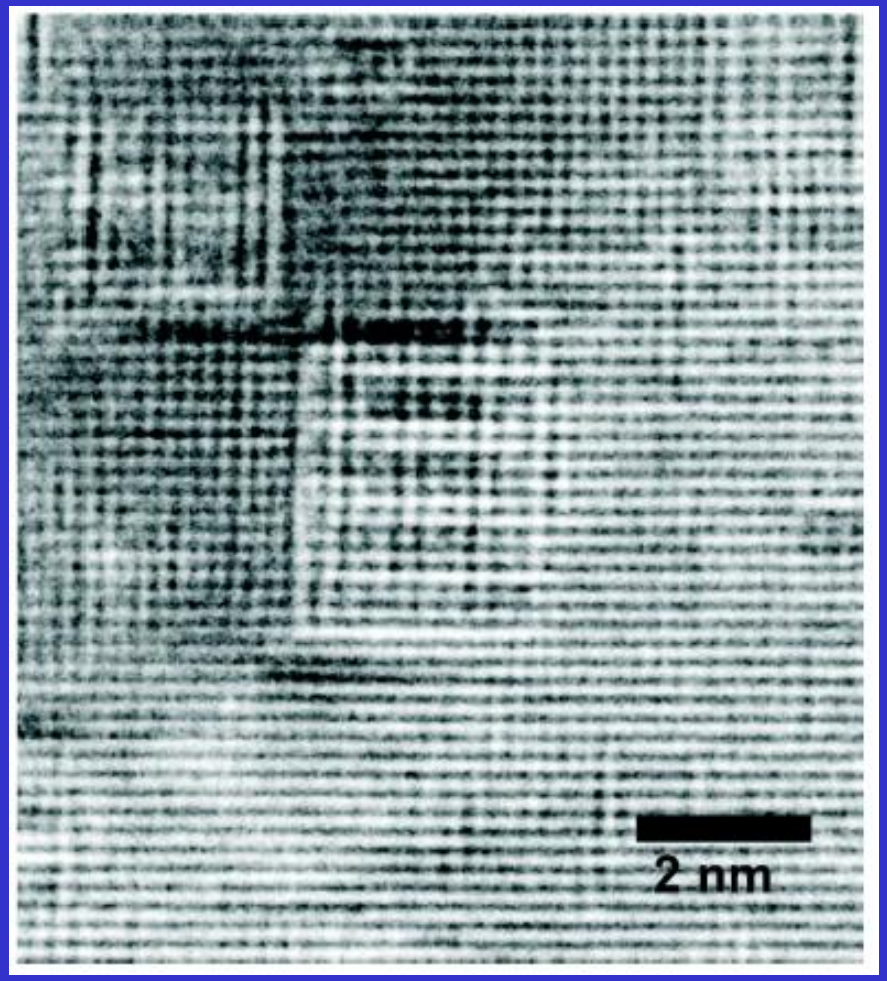

- Solid Kr nanoclusters at a depth of 75–120 nm with Moire´ fringes caused by the lattice mismatch between solid Kr and MgO.

High-resolution TEM image of a solid Kr nanocluster.

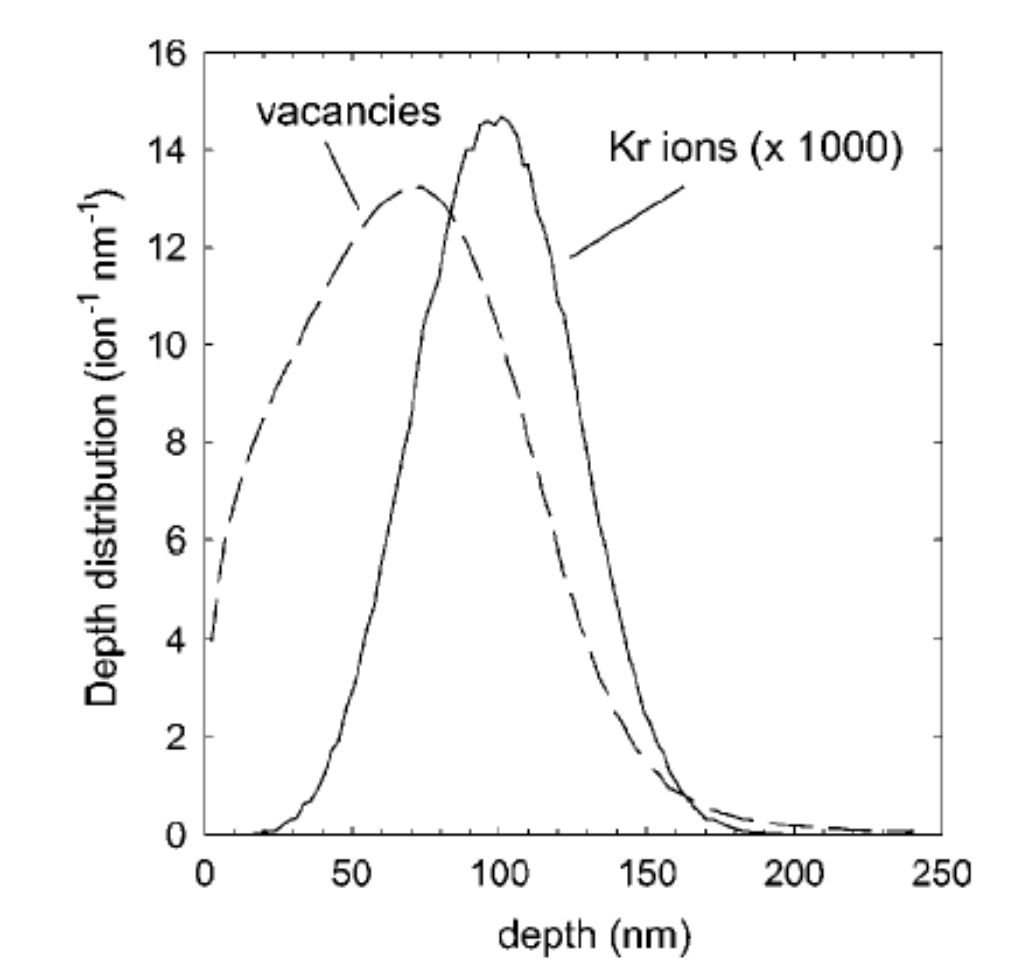

- Kr depth distribution (after implantation, prior to thermal anneal) and damage depth distribution as calculated using the SRIM2000 code.

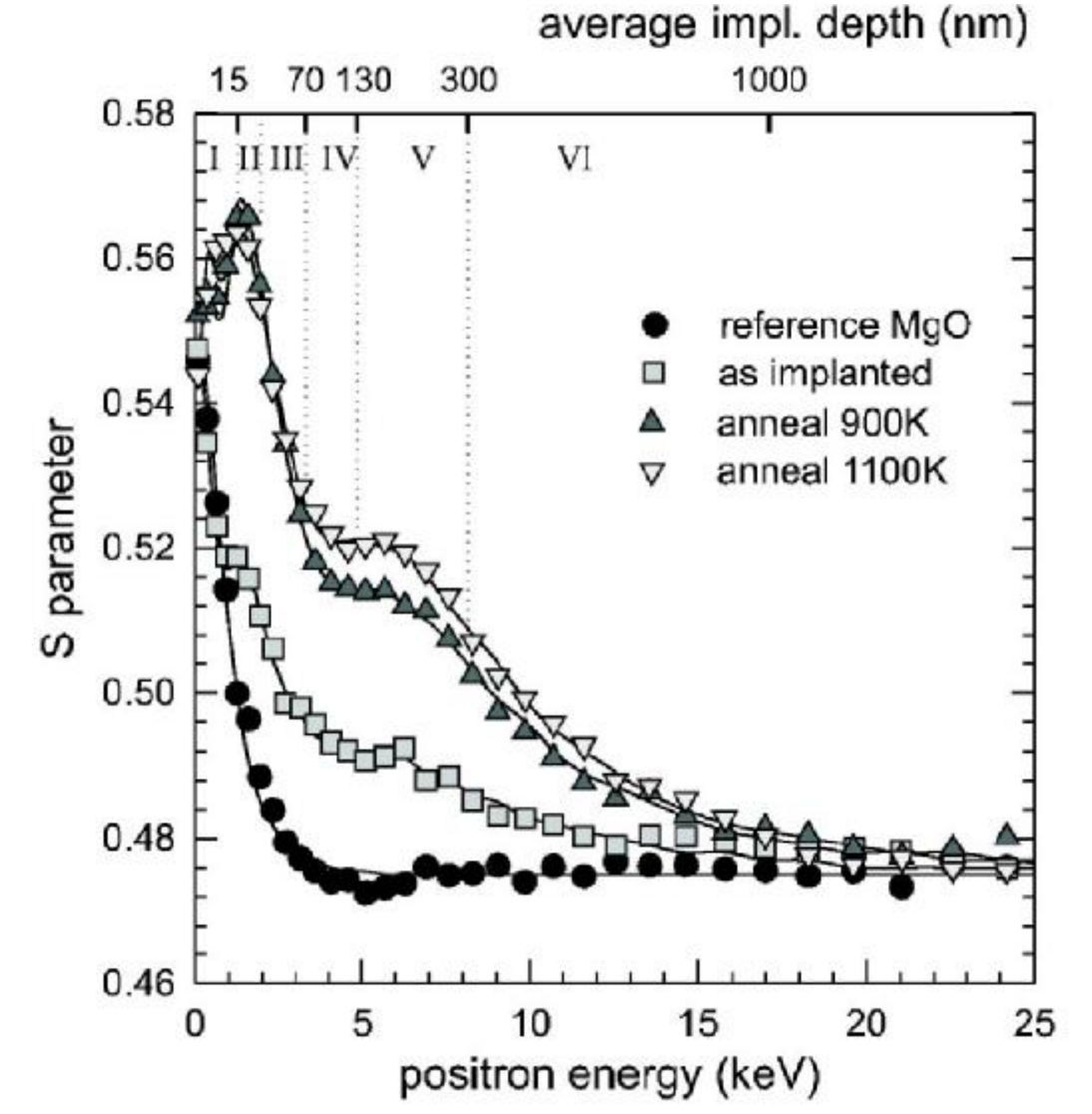

- *S* parameter vs positron energy measured for reference MgO and for MgO:Kr after implantation and after thermal annealings.

TABLE II. Model used for VEPFIT simulation. Note that the S parameters of layers I, III, and V are fitted with the same parameter.

Layer	Description	Depth (nm)	S par.	Diff. length (nm)
I	MgO with defects	0–15	S_{def} (fitted)	5
II	nanovoids	15–30	S_{voids} (fitted)	5
III	MgO with defects	30–70	S_{def} (fitted)	5
IV	Kr clusters	70–130	S_{Kr} (fitted)	5
V	MgO with defects	130–300	S_{def} (fitted)	20
VI	MgO bulk	>300	$S_{MgO}=0.475$	100

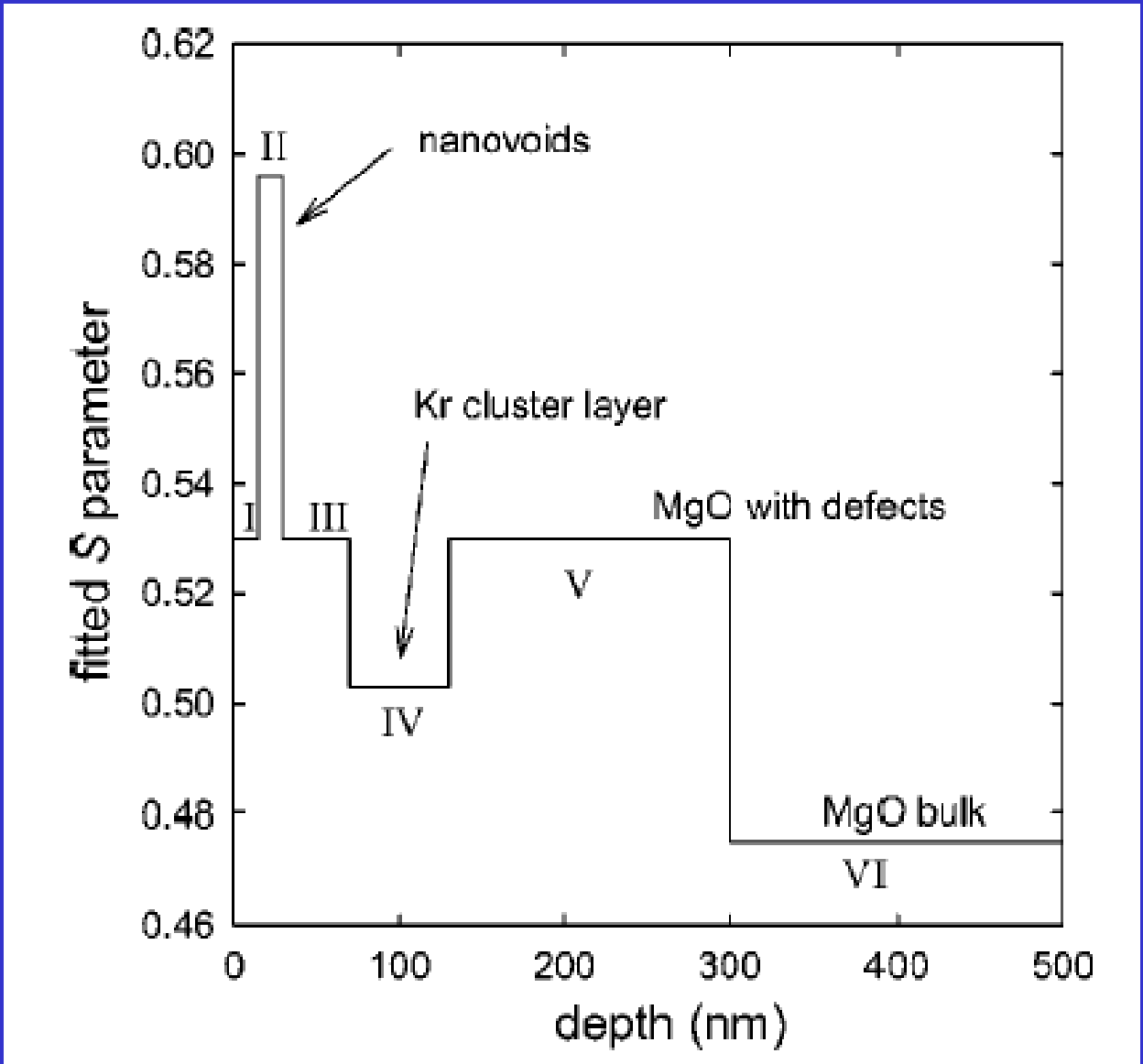

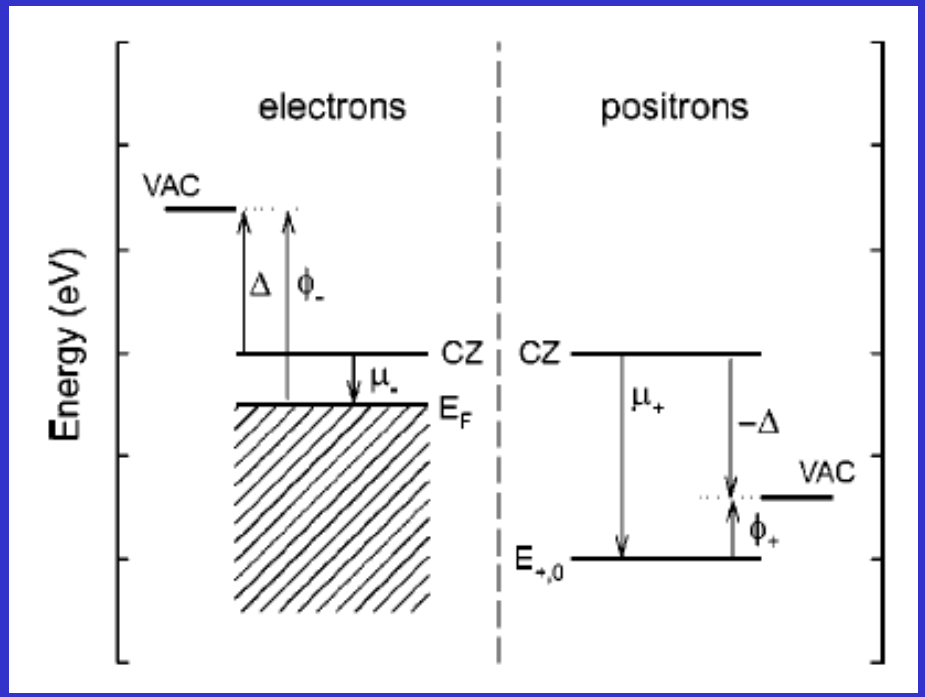

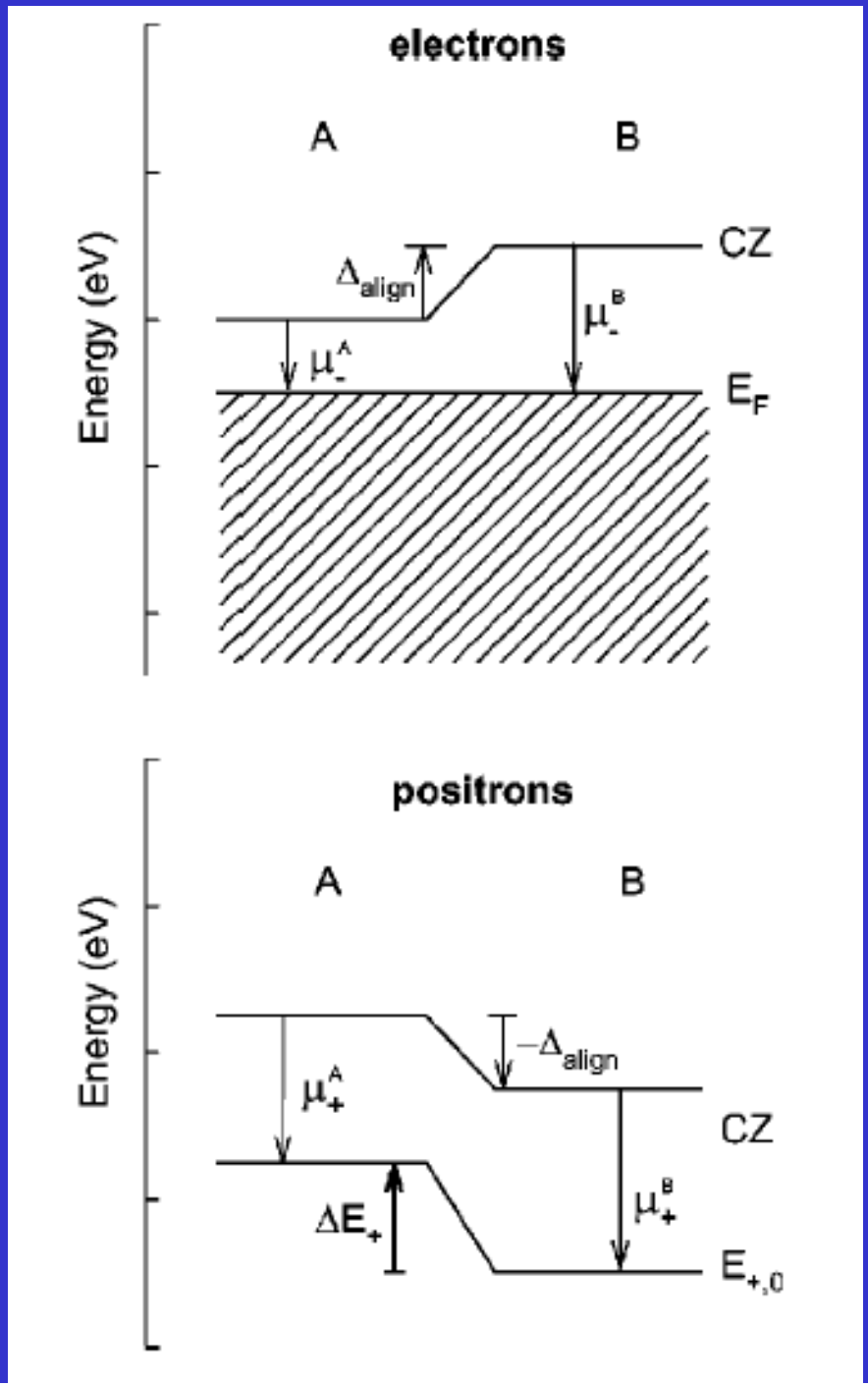

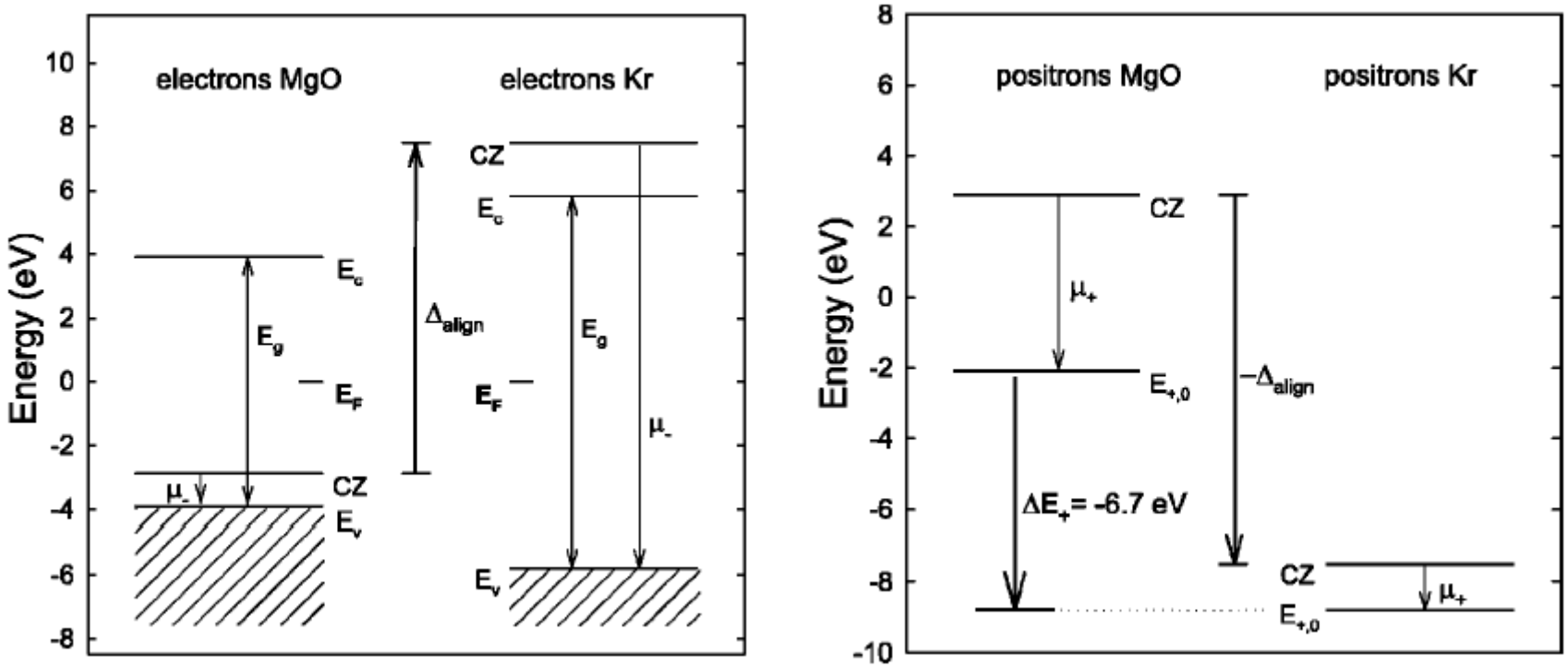

TABLE IV. Positronic potential difference between the Kr cluster and MgO in contact assuming alignment of the Fermi levels in metals [Eq. (6)], in insulators [Eq. (9)], or assuming alignment of the vacuum levels [Eq. (11)]. The data of Table III have been used to calculate the numerical values.

Level alignment	$\Delta E = E_+^{Kr} - E_+^{MgO}$	Result (eV)
Fermi (metals)	$\Delta E_+^{METAL} = (\mu_+^{Kr} + \mu_-^{Kr}) - (\mu_+^{MgO} + \mu_-^{MgO})$	NA [a]
Fermi (insulators)	$\Delta E_+^{INS} = (\mu_+^{Kr} + \mu_-^{Kr} + \frac{1}{2}E_g^{Kr}) - (\mu_+^{MgO} + \mu_-^{MgO} + \frac{1}{2}E_g^{MgO})$	-6.7 ± 1.5
Vacuum	$\Delta E_+^{VAC} = (-\phi_+^{Kr}) - (-\phi_+^{MgO})$	-0.5 ± 1.5

[a]Not applicable: Does not apply to the MgO‖Kr insulator-insulator interface.

二. 纳米粒子在表面

Thanks